Assessment of the spatio-temporal variability of the added value on precipitation of convection-permitting simulation over the Iberian Peninsula using the RegIPSL regional earth system model

Namendra Kumar Shahi, Jan Polcher, Sophie Bastin, Romain Pennel, Lluís Fita

Climate Dynamics
https://doi.org/10.1007/s00382-022-06138-y

Assessment of the spatio-temporal variability of the added value on precipitation of convection-permitting simulation over the Iberian Peninsula using the RegIPSL regional earth system model

Namendra Kumar Shahi[1] · Jan Polcher[1] · Sophie Bastin[2] · Romain Pennel[1] · Lluís Fita[3]

Received: 26 April 2021 / Accepted: 3 January 2022

Abstract
In this study, we have assessed the added value on the spatio-temporal distribution of the precipitation of convection-permitting simulation (3 km) compared to the parent coarse-scale parameterized convection simulation (20 km) with the high-resolution observational datasets i.e., SPREAD (5 km) and IBERIA01 (10 km) over the Iberian Peninsula (IP) in all four seasons during 2000–2009. Both simulations are evaluation runs based on ERA-Interim reanalysis and performed with the RegIPSL regional earth system model in the frame of the European Climate Prediction system (EUCP) H2020 project and COordinated Regional climate Downscaling Experiment (CORDEX). We have not found significant improvement in the convection-permitting simulation compared to the parent coarse-scale simulation for the seasonal mean precipitation of the IP except the spatial variation over mountainous peaks. The kilometer-scale simulation significantly underestimates the observed seasonal mean precipitation over the western parts of the IP compared to the coarse-scale simulation, which may be attributed to a change of local dynamics in the kilometer-scale simulation with a weakening and southward shift of the moisture-laden westerly winds approaching from the Atlantic Ocean over the IP (i.e., a decline in atmospheric moisture transport from the Atlantic Ocean towards the IP). However, the added value of kilometer-scale simulation over the driving coarse-scale simulation is obtained for various indices; in the representation of the spatio-temporal distribution of the wet-day precipitation frequency and intensity, and the extreme/heavy precipitation events for each season at both resolutions i.e., downscaled and upscaled. It has also been noted that the spatio-temporal distribution of precipitation for all metrics used varies between the two observational datasets for all seasons.

Keywords Added value · Dynamical downscaling · RegIPSL model · Convection-permitting simulation · Precipitation events

1 Introduction

Regional climate models (RCMs) have proven to be a powerful/useful tool for dynamically downscaling the coarse-scale information/datasets at the regional-to-local scale (Prein et al. 2015). The coarse-scale information is handed over to a RCM via the lateral boundaries, and the information is usually provided from either general circulation models (GCMs), reanalysis, or large-scale regional models. In the last two–three decades, the RCMs have been used for improving our understanding of regional climate processes of different parts of the world and used for impact assessment studies. Also, considerable efforts have been/are being made to further advance and improve the RCMs by increasing their complexity and resolution through the CORDEX program (Jacob et al. 2014; Ruti et al. 2015). Recent advances in computing power/resources have allowed limited-area RCMs to be run at kilometer-scale grid spacing. Increasing the spatial resolution towards convection-permitting scales (<4 km; also known as convection-permitting/resolving/allowing; Weisman et al. 1997) can resolve deep convection explicitly on the model grid without the need

✉ Namendra Kumar Shahi
nkshahi2010@gmail.com;
namendra-kumar.shahi@lmd.polytechnique.fr

[1] Laboratoire de Météorologie Dynamique (LMD), CNRS-IPSL, École Polytechnique, 91128 Palaiseau, France

[2] LATMOS/IPSL, UVSQ Université Paris-Saclay, CNRS, Sorbonne Universite, Guyancourt, France

[3] Centro de Investigaciones del Mar y la Atmósfera (CIMA), CONICET-UBA, CNRS-IRD-CONICET-UBA IRL-3351 IFAECI, Buenos Aires, Argentina

Published online: 17 January 2022

for a convective parametrization scheme (Hohenegger et al. 2008; Kendon et al. 2012, 2017; Prein et al. 2015). As several studies have shown that the parameterizations of sub-grid scale convection are a key source of errors and uncertainties in the climate model simulations (Bechtold et al. 2004; Randall et al. 2007; Déqué et al. 2007; Hohenegger et al. 2008; Brockhaus et al. 2008). Also, increasing resolution leads to a better representation of orography and land surface fields which are crucial for the initiation of convection in complex terrain (Hohenegger et al. 2008; Kendon et al. 2012; Chan et al. 2013; Ban et al. 2014), and also provides a step-change in our capability for understanding future climate change at local to regional scale and for and high-impact extreme weather events that greatest impact society (Rasmussen et al. 2020; Helsen et al. 2020; Kendon et al. 2014, 2019, 2021).

Over the last decade, several studies have demonstrated the clear benefits and added value of the convection-permitting models in the simulation of precipitation characteristics with much greater realism, including the diurnal cycles, spatial distribution of precipitation, intensity and frequency distribution, and extremes compared to the coarse-scale model (Prein et al. 2015; Meredith et al. 2015; Fosser et al. 2015; Lind et al. 2016, 2020; Brisson et al. 2016; Liu et al. 2017; Leutwyler et al. 2017; Zittis et al. 2017; Karki et al. 2017; Berthou et al. 2018; Fumière et al. 2019; Broucke et al. 2019; Li et al. 2019, 2021; Chang et al. 2020; Knist et al. 2020; Kouadio et al. 2020; Coppola et al. 2020; Zhou et al. 2021; Ban et al. 2021).

Some recent coordinated efforts towards a better understanding of the regional climate modelling at kilometer resolutions are undergoing like; the dedicated Coordinated Regional Downscaling Experiment Flagship Pilot Studies (CORDEX-FPS; https://cordex.org/experiment-guidelines/flagship-pilot-studies/) on Convective phenomena at high-resolution over Europe and the Mediterranean and also within the European Climate Prediction System (EUCP; https://www.eucp-project.eu/). Within these projects, several regional modelling groups across Europe are conducting climate simulations in a common greater Alpine domain with horizontal resolutions around 3 km, with the aim to generate/build multi-model ensembles of simulations at the convective-permitting scales over a decade-long period to explore the capabilities and uncertainties of the convection-permitting model simulations in a systematic manner for present and future climates (Coppola et al. 2020; Ban et al. 2021; Pichelli et al. 2021). The ensemble of ERA-Interim driven present-day convection-permitting climate simulations have shown superior performance in simulating the precipitation characteristics compared to coarse-resolution climate simulations, although differences between the kilometer-scale simulations and observations still exist (Coppola et al. 2020; Ban et al. 2021). Panosetti et al. (2019) have shown that the kilometer-scale simulations are climatologically more robust in case of strong orographic forcing (domain over the European Alps) and less robust in central German.

Keeping in mind the usage and added value of convection-permitting model simulations in the above literature, here we evaluate the added value of the convection-permitting/resolving simulation (3 km resolution) compared to the coarse-resolution parameterized convection simulation (20 km resolution) in the representation of the spatio-temporal pattern of the observed mean and extreme precipitation over the Iberian Peninsula for all four seasons [i.e. December–January–February (DJF; Winter), March–April–May (MAM; Spring), June–July–August (JJA; Summer), and September–October–November (SON; Autumn)] for the period of 2000–2009. Both simulations are based on the ERA-Interim reanalysis (Dee et al. 2011) and have been performed using a recently developed regional climate model called RegIPSL by the Institut Pierre Simon Laplace (IPSL, https://gitlab.in2p3.fr/ipsl/lmd/intro/regipsl/regipsl/-/wikis/home) group in the frame of the European Climate Prediction system (EUCP) H2020 project and COordinated Regional climate Downscaling Experiment (CORDEX), and details about this model and simulations are given in the next section. The simulated precipitation is evaluated with the available high-resolution observational gridded datasets i.e., SPREAD (5 km) and IBERIA01 (10 km). In the comparison of the model-simulated results with observations, the uncertainty associated with the observational datasets especially over mountainous regions due to the sparseness of rain gauge stations at high elevations must be taken into account (Sevruk 1985; Frei et al. 2003). Recent studies actually report that total annual precipitation can be better represented by well-configured high-resolution atmospheric models in mountainous terrains, than with spatial estimates derived from observational products (Lundquist et al. 2020).

The research paper is mainly structured into three sections. In Sect. 2, we have presented a detailed description of the model configuration for the two simulations, as well as observational datasets used for validation and methodology used. A detailed analysis of the added value of the fine-scale simulation over the driving coarse-scale simulation against the observations is presented in Sect. 3, and finally, the summary and conclusions are given in Sect. 4.

2 Model simulations, data, and methodology

2.1 Model simulations and data

In the frame of the EUCP H2020 project and CORDEX, we have performed the ERA-Interim driven regional climate simulations with the coupled atmosphere-land RegIPSL model over the European domain at 20 km horizontal resolution (EUR20; with parameterized convection) and also over the European South-West domain at 3 km (SWE3; convection-permitting/resolving) horizontal grid spacing

for the period of 1999–2009 (the first year period has been used as a model spin-up). The details of the model configuration and the WRF physical schemes are given in Table 1. The European South-West domain (i.e., Iberian Peninsula) is an area with a rich diversity of climates that is affected by several high-impact extreme events such as droughts and flash floods, for which the coupling processes between the land surface and the atmosphere play an important/key role. The experiment is performed as a chain of simulations while the EUR20 simulation is forced by the 6-hourly ERA-Interim initial and lateral boundary conditions (IC-LBCs) and the SWE3 simulation is forced by the 3-hourly EUR20 simulated IC-LBCs. The model domain with terrain height in the meters for the EUR20 and SWE3 simulations is shown in Fig. 1a, b, respectively.

The RegIPSL is a newly developed regional earth system model and is maintained at the Institut Pierre Simon Laplace (IPSL). The atmospheric component of the RegIPSL model is WRF (Weather Research and Forecasting; Skamarock et al. 2008; Fita et al. 2019) model, which is coupled to the ORCHIDEE (Organising Carbon and Hydrology in Dynamic Ecosystems; Krinner et al. 2005) land-surface model and NEMO (Nucleus for European Modelling of the Ocean; Madec et al. 1998) ocean model. We have used the OASIS coupler (https://portal.enes.org/oasis) for coupling, and XIOS (or XML I/O Server, http://forge.ipsl.jussieu.fr/ioserver) libraries are used for the management of the input/output.

The high-resolution SPREAD (5 km; Serrano-Notivoli et al. 2017) and IBERIA01 (10 km; Herrera et al. 2019) daily gridded mean precipitation observational datasets have been used as reference datasets for the validation of the model simulated precipitation. The SPREAD dataset is based on the 12,858 observatories and is available at land points of Spain, while the IBERIA0 is based on a total of 3761 rain gauge stations and covers the landmass of Spain as well as Portugal. A detailed description of these datasets can be found from the references given above.

2.2 Methodology

First, we evaluate the added value of SWE3 in the spatio-temporal distribution of seasonal mean precipitation and also focus on the altitudinal variations of mean precipitation. We also examine the atmospheric conditions to explain the differences observed in seasonal mean precipitation between the two simulations (a detailed discussion on this is given in Sect. 3.2). In the second step, we examine the added value of SWE3 in the spatial/altitudinal distribution of the wet-day precipitation frequency and intensity of daily mean precipitation. A wet day is a day with precipitation ≥ 1 mm. We also use the probability density function (PDF) to showcase the overall distribution of daily precipitation intensity, and Kolmogorov–Smirnov (K–S) goodness-of-fit test is used to measures the dissimilarity/distance between the two samples i.e., model and observed precipitation (Chakravarty et al. 1967; Torma et al. 2015; Shahi et al. 2021). The KS distance is defined as the maximum vertical absolute difference between two empirical cumulative distribution functions (ECDFs). The K–S distance varies between zero (perfect overlap between the two distributions) and one (no overlap between the two distributions). It is calculated from the formula:

$$d_{KS}(F, G) = supr_{t \in R} |F(G) - G(t)|$$

Table 1 Description of model configurations

Description	Selection	
	EUR20 simulation	SWE3 simulation
WRF version	3.7.1	3.7.1
Dynamic solver	ARW	ARW
Horizontal grid spacing	20 km	3 km
Grid dimensions	301 × 193	581 × 651
Vertical levels	46 (top 50 hPa)	46 (top 70 hPa)
Integration time	90 s	10 s
Radiation (shortwave and longwave)	RRTMG Scheme (integration timestep = 30 min)	RRTMG Scheme (integration timestep = 5 min)
Microphysics	WRF single-moment (WSM) 5-class scheme	Thompson scheme
Atmospheric surface layer	MYNN surface layer	MYNN surface layer
Land surface	ORCHIDEE	ORCHIDEE
Planetary boundary layer (PBL)	MYNN 2.5 level TKE scheme	MYNN 2.5 level TKE scheme
Cumulus	Kain–Fritsch scheme	No cumulus scheme is used

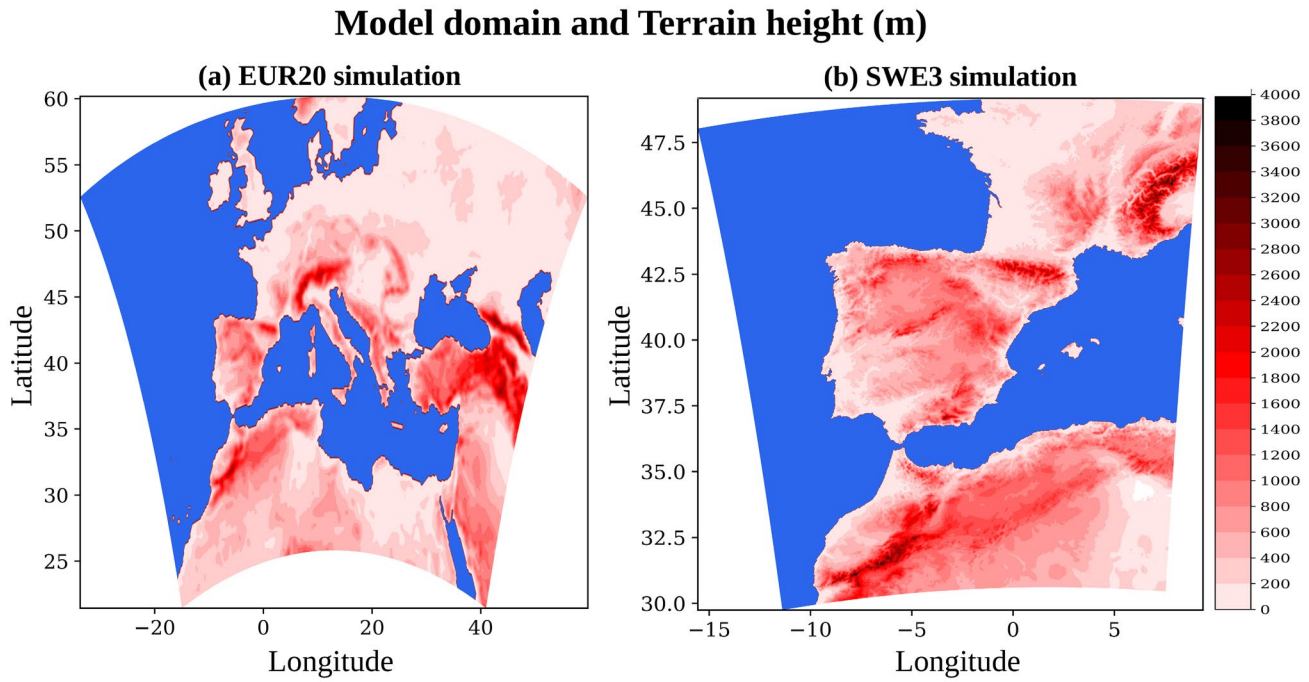

Fig. 1 Model domain with terrain height in the meters for the **a** EUR20, and **b** SWE3 simulations. The blue colour represents the ocean

where F and G are the two ECDFs and *supr* represents the supremum function (Chakravarty et al. 1967; Torma et al. 2015).

In the final evaluation step, we focus on the representation (spatial/altitudinal) of heavy/extreme precipitation. Basically, we used two climate extreme indices i.e., R99p and Rx1day (Karl et al. 1999; Peterson 2005). The R99p is the 99th percentile of the mean precipitation, and Rx1day is the highest one-day precipitation amount.

We use the Taylor diagram (Taylor 2001) to assess the performance of both simulations in representing the spatial distribution of precipitation (for all cases/indices). We constructed the Taylor diagram with the results of the spatial Index of Agreement (instead of the spatial correlation coefficient) and normalized standard deviation. Willmott (1982) stated that the correlation coefficient is often a misleading measure of accuracy, and proposed a new skill metric i.e., index of agreement (IOA). The IOA is calculated as follows:

$$IOA = 1 - \frac{\sum_{i=1}^{n}\left(M_i - O_i\right)^2}{\sum_{i=1}^{n}\left(\left|M_i - \overline{O}\right| + \left|O_i - \overline{O}\right|\right)^2}$$

where M and O represent the model and observation, respectively. $\overline{O}$ represents the observed mean value and n is the number of total data/grid points. The IOA is bounded between 0 and 1, where a value close to 1 indicates more efficient forecasting skills.

We have used two observational daily gridded datasets of different resolutions [i.e., SPREAD (5 km) and IBERIA01 (10 km)] for the validation of the simulated precipitation. When dealing with the observations of precipitation, one must take into account the shortcomings associated with them (Sevruk 1985; Frei et al. 2003; Isotta et al. 2014; Prein and Gobiet 2017), like: (i) underestimation of precipitation, especially over mountainous regions due to the sparseness of rain gauge stations at high elevations; (ii) wetting and evaporation losses; and (iii) the wind-induced rain gauge undercatch. Additionally, different interpolation methods are used in the production of these datasets, which may result in systematic biases. These biases mainly include underestimation of high intensities (smoothing effect) and overestimation of low intensities (moist extension into dry areas) (Isotta et al. 2014).

To make the results comparable, we have validated the SWE3 simulation with the closest resolution observation only (i.e., SPREAD), and the SWE3 precipitation is upscaled before the analysis to a SPREAD grid [5 km; in Figs. 4(a1–d1), 8(a1-d1), 9(a1-d1), 10, 11, 14(a1–a4), S1(a1–a4), S6(a1–d1), and S7(a1–d1)]. To see the added value of the SWE3 over the EUR20, all the precipitation datasets (both observations and SWE3) are upscaled before the analysis to a EUR20 grid [20 km; in Figs. 4(a2–d2), 5, 6, 8(a2–d2), 9(a2–d2), 12, 13, 14/S1 (from the second horizontal panel), S2, S4, S6(a2–d2), and S7(a2–d2)]. In Figs. 1,

2, 3, 7, and 15, the data are presented on their original grid. For more clarity and to avoid confusion, we have mentioned the details of the figure before the discussion in each section.

3 Results and discussion

3.1 Spatio-temporal distribution of mean precipitation

In this section, we evaluate the spatial distribution of the simulated 10-year seasonal (DJF, MAM, JJA, and SON) mean precipitation over the Iberian Peninsula (IP). The seasonal mean precipitation from the SWE3, EUR20, SPREAD, and IBERIA01 is shown in Fig. 2a1–a4, b1–b4, c1–b4, and d1–d4, respectively. The relative bias in seasonal mean precipitation of the SWE3 is calculated for each season against the closest resolution observation only (i.e., SPREAD) on SPREAD grid (SWE3 precipitation is upscaled on SPREAD grid) as shown in Figs. S1(a1–a4). To see the added value of the SWE3 over the EUR20, we have upscaled all the precipitation datasets (both observations and SWE3) to the lowest resolution (i.e., EUR20 grid) and then we have calculated the biases. The relative bias in seasonal mean precipitation of the SWE3 and EUR20 is estimated against the SPREAD [IBERIA01] on the EUR20 grid and is shown in Fig. S1(b1–b4) [S1(d1–d4)] and S1(c1–c4) [S1(e1–e4)], respectively. The relative difference in seasonal mean precipitation between SPREAD and IBERIA01 on the EUR20

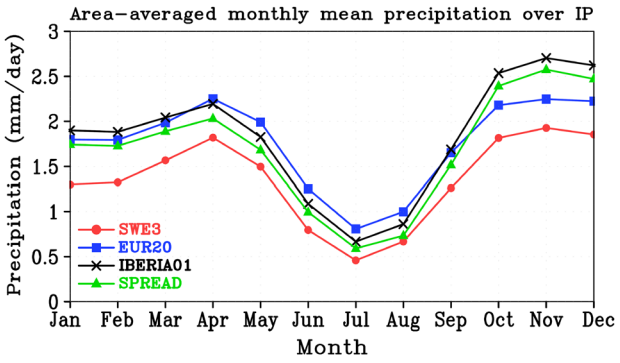

Fig. 3 Annual cycle of area-averaged monthly mean precipitation over the Iberian Peninsula (IP, over the area of the SPREAD observation) from the SWE3 (red), EUR20 (blue), IBERIA01 (black), and SPREAD (green) during 2000–2009. Units are in mm day^{-1}

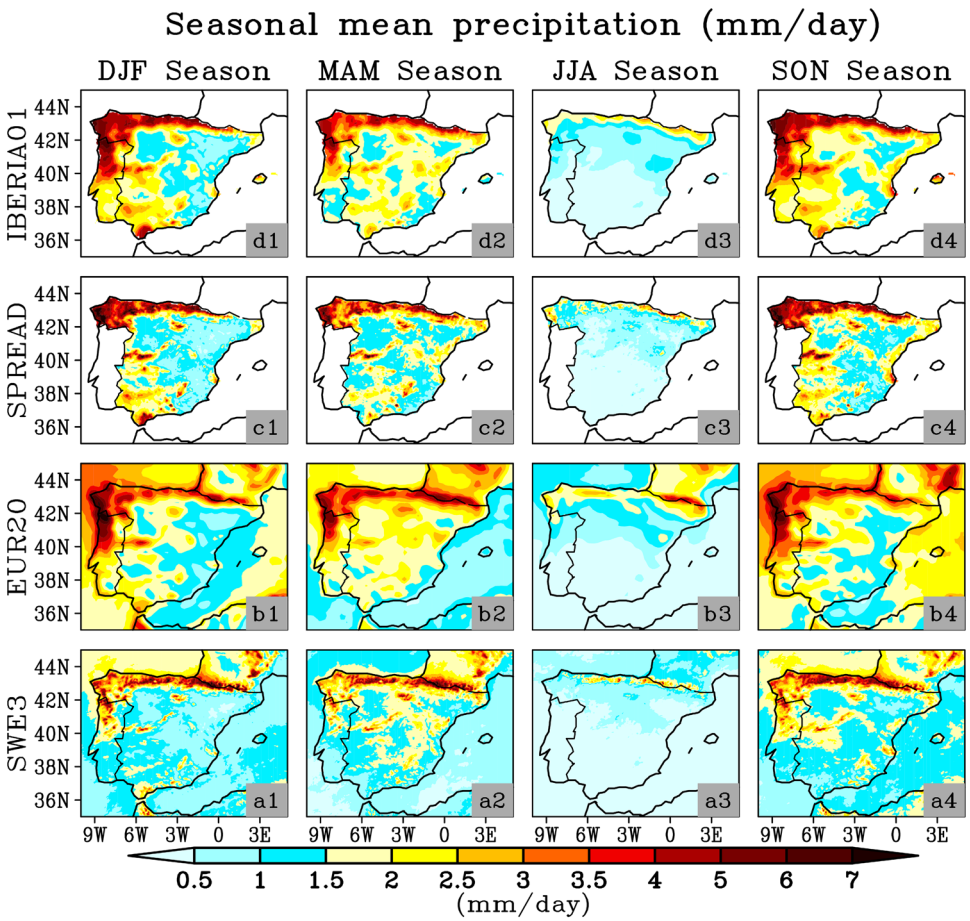

Fig. 2 The 10-year (2000–2009) climatological seasonal (DJF, MAM, JJA, and SON) mean precipitation from the **a1–a4** SWE3, **b1–b4** EUR20, **c1–c4** SPREAD, and **d1–d4** IBERIA01, respectively. Units are in mm day^{-1}

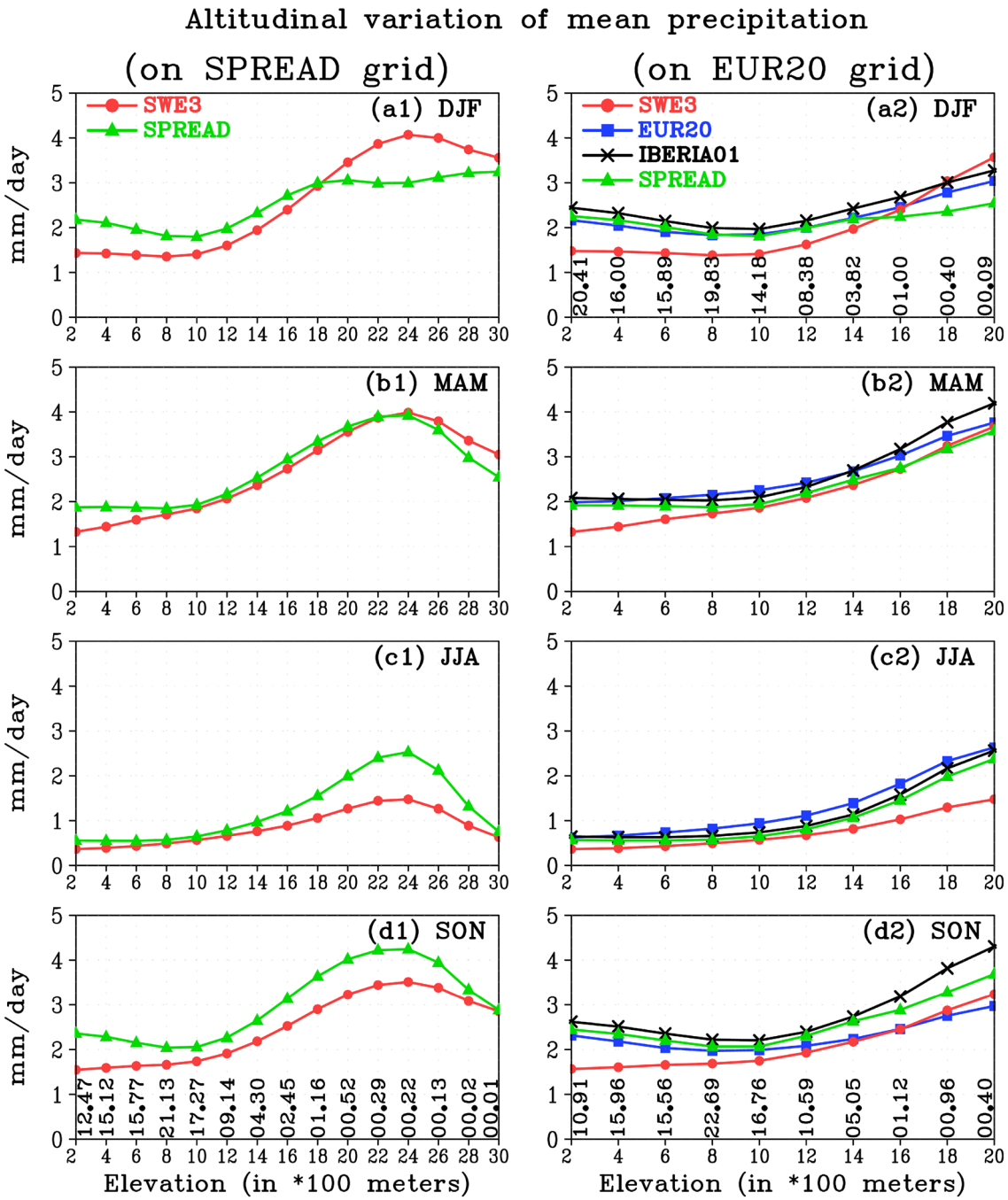

Fig. 4 Altitudinal distribution of the mean precipitation from the SWE3 (red), EUR20 (blue), IBERIA01 (black), and SPREAD (green) over the Iberian Peninsula (IP, over the area of the SPREAD observation) on the SPREAD & EUR20 grids for the **a1**, **a2** DJF, **b1**, **b2** MAM, **c1**, c**2** JJA, and **d1**, **d2** SON seasons during 2000–2009. The percentage of the total grid points covered by each class on the **d1** SPREAD and **d2** EUR20 resolutions is also shown. x-axis panels represent the elevation class of 200 m. The percentage of actual number of rain gauge stations presented in the IBERIA01 dataset is also shown in a2. Units are in mm day^{-1}

grid is also calculated for each season and is shown in Fig. S1(f1–f4).

The observed climatological seasonal mean pattern shows that the highest precipitation occurs over the northwestern and northern regions of the IP in all seasons (Fig. 2). As can be seen from Fig. 2, the regional to local scales precipitation pattern with maximum precipitation in the mountainous peaks of the study domain has been produced by kilometric-scale simulation (SWE3; a1–a4) compared to the coarse-scale simulation (EUR20; b1–b4) for all four seasons.

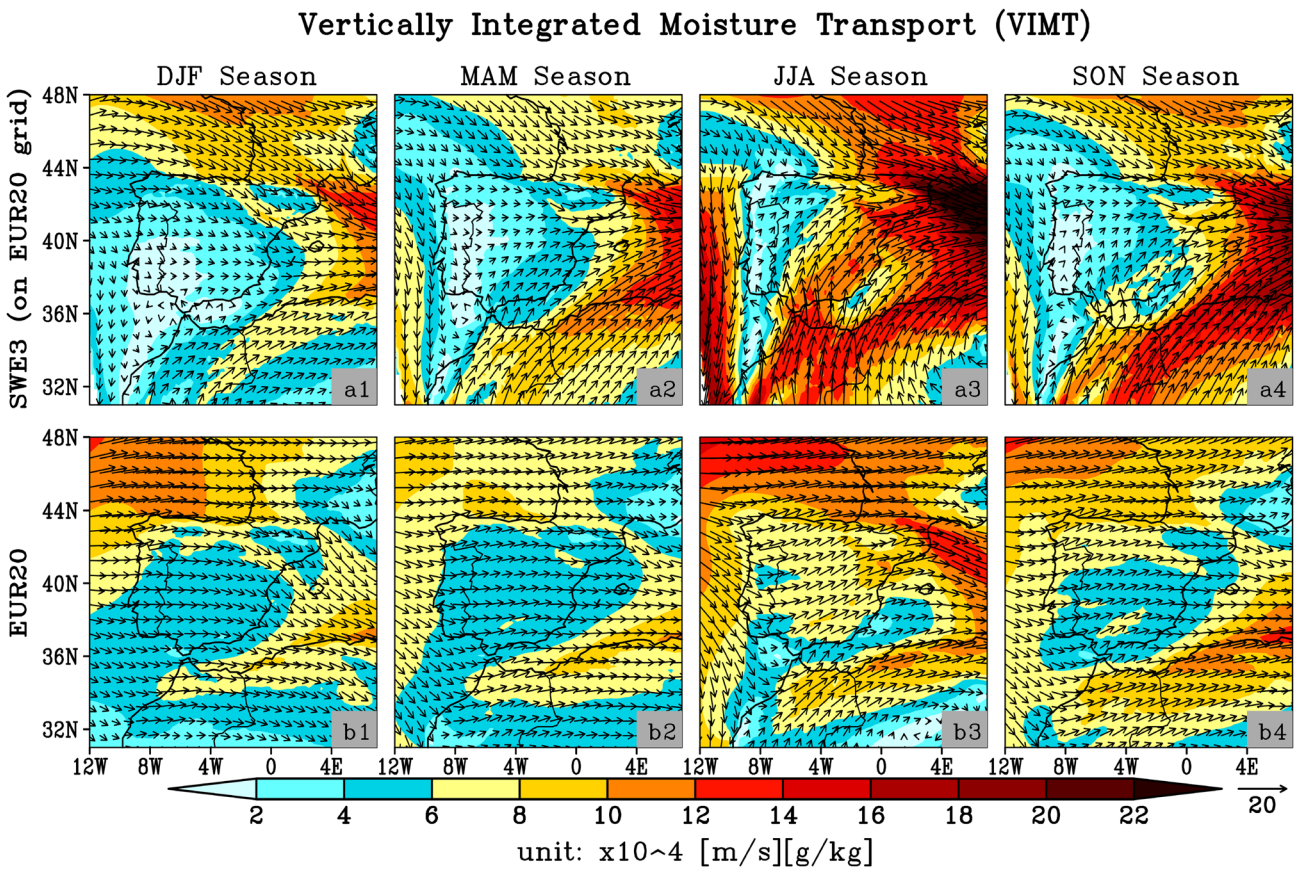

Fig. 5 The seasonal (DJF, MAM, JJA, and SON) mean vertically integrated (from surface to 300 hPa) moisture transport from the **a1**–**a4** SWE3 on the EUR20 grid, and **b1**–**b4** EUR20, respectively. The shaded color represents the magnitude of the wind, and the vectors represent the wind direction. Units are in $\times 10^4$ [m/s] [g/kg]

However, the SWE3 simulation exhibits less precipitation in almost all areas of the IP (including the surrounding oceans) except for hilly peaks compared to the EUR20 simulation, and perhaps it may be related to improper lateral boundary conditions (LBCs from EUR20), as it is possible that the LBCs (large-scale forcing fields) used for the SWE3 simulation may already have biases that can propagate in the SWE3 simulation domain. Several studies have shown that the biases existing in the LBCs affect the entire limited-area regional climate models (RCMs) domain (Warner et al. 1997; Rinke and Dethloff 2000; Wu et al. 2005; Diaconescu et al. 2007; Køltzow et al. 2008; Diaconescu and Laprise 2013; Brisson et al. 2015; Panosetti et al. 2019; Rocheta et al. 2014, 2020; Ahrens and Leps 2021). However, any biases already in the LBCs can influence the performance of SWE3, but the reduced precipitation compared to EUR20 cannot be addressed only to LBCs errors. The already mentioned issue of the RCM using cumulus parameterizations (ex. EUR20) tending to over-trigger convection, is usually partially corrected at the convection-permitting scale (SWE3). In the next section, we try to understand all this and provide some dynamical factors. On the other hand, a better representation of the topography of mountainous regions in the SWE3 simulation allows the realistic local mountain-valley circulation and other local-scale processes that lead to a better representation of the precipitation in these areas (Karki et al. 2017).

As can be seen from Fig. S1, the bias patterns derived from the simulations against both observations are more or less similar to each other in terms of variability with slight differences in magnitude at some locations for all seasons. On the other hand, we have also noted that the intensity of precipitation varies slightly between the two observations for all seasons which explains the above-noticed differences, as the IBERIA01 shows slightly higher precipitation than the SPREAD in almost all regions of the IP (SPREAD is drier; Fig. S1f1–f4), and this may be due to the different resolutions of both observational datasets but also to other factors such as the number of stations used and the methods of interpolation used in building these datasets. However, a noticeable difference is observed between the two observations in

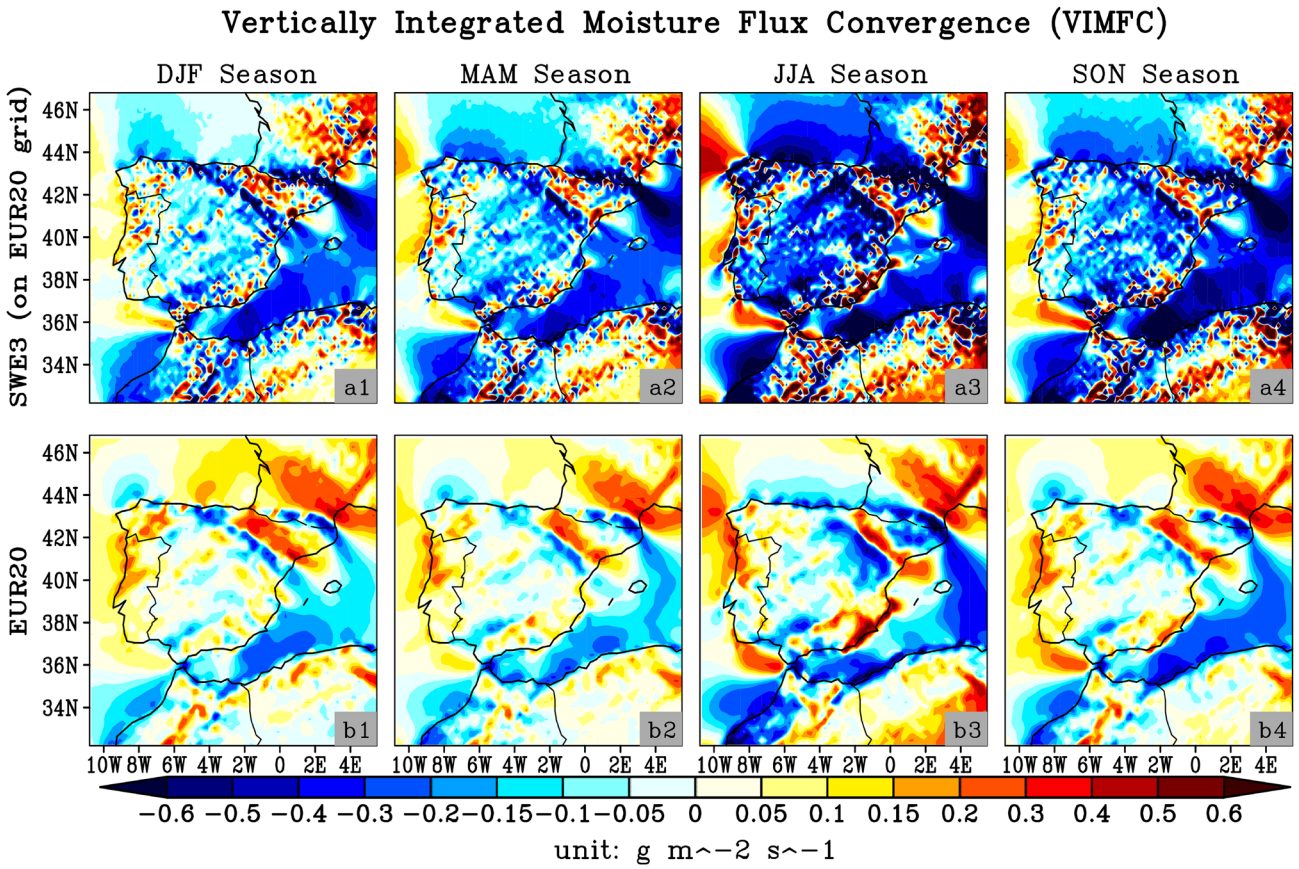

Fig. 6 The seasonal (DJF, MAM, JJA, and SON) mean vertically integrated (from surface to 300 hPa) moisture flux convergence from the **a1–a4** SWE3 on the EUR20 grid, and **b1–b4** EUR20, respectively. Units are in g m^{-2} s^{-1}

the eastern and southern parts of the IP for the DJF and JJA seasons, respectively (Fig. S1f1, S1f3).

The bias pattern of the SWE3 against the SPREAD on a finer-scale grid (i.e., on the SPREAD grid) provides detailed regional to local scales information (Fig. S1a1–a4), although the pattern is similar to the coarse-scale grid (i.e., on the EUR20 grid) bias pattern (Fig. S1b1–b4). The SWE3 simulation shows a dry bias of up to 60% (80% for the JJA) in observed seasonal mean precipitation especially over the western regions of the IP for all seasons (Figs. S1b1–b4, S1d1–d4), whereas the EUR20 simulation exhibits relatively low wet precipitation bias over the maximum areas of the western regions of the IP for the MAM and JJA seasons (Figs. S1c2–c3, S1e2–e3) and the mixture of dry and wet precipitation biases are observed in these areas for SON and DJF seasons (Figs. S1c4–c1, S1e4–e1). On the other hand, the SWE3 simulation slightly overestimates the observed seasonal mean precipitation in some parts of the mountainous ranges of the IP for the MAM and SON seasons, whereas in the DJF season, overestimation of precipitation is noted only in the peaks of the mountains ranges. For the JJA season, the SWE3 substantially underestimates the observed mean precipitation over eastern parts of the IP and overestimates the precipitation over the south-central parts of the IP and also in some parts of the central and northern plateau mountainous regions of the IP. However, due to the sparse station densities in the mountainous regions, there is considerable/larger uncertainty in the observational datasets that may explain the bias of the mountainous regions in the simulations. From the above discussion, it can be concluded that SWE3 has a greater tendency to produce larger dry bias across IP than EUR20, and severely underestimated the observed mean precipitation especially in the western parts of the IP.

We have also calculated the annual cycle of area-averaged monthly mean precipitation over the Spain landmass (over the area of the SPREAD) as shown in Fig. 3. It can be clearly seen from Fig. 3 that the SWE3 simulation underestimates the observed mean precipitation of each month, while the EUR20 simulation is more in agreement with the observed monthly mean precipitation except in the fall. The SWE3 simulation underestimates the precipitation by about 0.7 mm/day in October–March, while EUR20 simulated

precipitation is much closer to the observations in January–March and underestimates the precipitation by about 0.3 mm/day in October–December (Fig. 3). It is also noted that the SWE3 (EUR20) slightly underestimates (overestimates) the precipitation in April-September (Fig. 3). It is clear from the above discussion that the SWE3 worsened the result in the case of mean precipitation. In other words, we have not observed the added value of convection-permitting simulation (i.e., SWE3) in the case of mean precipitation consistently with earlier studies (Prein et al. 2013, 2016; Warrach-Sagi et al. 2013; Kotlarski et al. 2014). These studies indicate that an increase of RCM resolution (convection-permitting scales) bears added value, but this added value can cancel out by larger spatial and temporal averaging. The impact of resolution on mean precipitation is also observed as the SPREAD shows slightly less precipitation than the IBERIA01 and this is true for all months (Fig. 3). However, the gridded observational datasets were not built with the same methodology and with the same number of stations, which can probably/potentially play a greater role in the discrepancies between the observational datasets than the resolution.

We have also calculated the season of highest precipitation over the IP to illustrate the precipitation cycle with associated phenomena as shown in Fig. S2. To make the results comparable, we have upscaled all the precipitation datasets (both observations and SWE3) before calculation to the lowest resolution grid (i.e., EUR20 grid; 20 km). The data obtained from the EUR20, SWE3, SPREAD, and IBERIA01 is shown in Figs. S2a, S2b, S2c, and S2d, respectively. The analysis shows the season of highest precipitation of individual simulations and observations. As we know, the IP receives the largest amounts of precipitation during the winter and autumn seasons, which mainly affects western and central Iberia and is originated mostly by synoptic low-pressure systems (i.e., depressions and frontal systems) approaching from the Atlantic Ocean (Serrano et al. 1999; Trigo and DaCamara 2000; Muñoz-Díaz and Rodrigo 2004; Vicente-Serrano and López-Moreno 2006; Herrera et al. 2010; Belo-Pereira et al. 2011; Rios-Entenza et al. 2014). Also, the maximum of precipitation around Mediterranean coastal regions during the autumn season is mainly associated with frontal activity in the Mediterranean. These aspects are well demonstrated by both high-resolution observational datasets (Fig. S2c, d). During spring and summer, local and mesoscale convective processes (terrestrial moisture; precipitation recycling) play a more relevant/active role in the modulation of Iberian precipitation (Belo-Pereira et al. 2011; Rios-Entenza et al. 2014). However, the seasonal mean precipitation in the summer season is much less than that of the other seasons, and this is also evident from the data (Fig. S2c, d). The eastern regions of the IP receive the relative maximum precipitation in the spring, which becomes the absolute maximum precipitation in the annual cycle (Fig. S2c, d). It can be seen from Fig. S2(a, b) that both simulations capture the observed patterns to a great extent, however, there are some differences in some places. The clear added value of convection-permitting simulation (SWE3) compared to the coarse-resolution simulation (EUR20) in the correct representation of the observed season (including area) of the highest precipitation over the Mediterranean coastal regions, southern and northern regions of the IP can be seen from the Fig. S2a, b. However, in the simulations, the areas with maximum precipitation during the spring season are more spread over the central regions than observed. Overall, SWE3 has shown better performance in simulating the observed regions with the highest precipitation of the season compared to EUR20.

For the quantitative analysis, the Taylor diagram (Taylor 2001) is constructed using the spatial Index of Agreement (IOA) and the normalized standard deviation (NSD) ratio between observed (i.e. SPREAD and IBERIA01) and simulated seasonal mean precipitation for each season as shown in supplementary Fig. S3a, b. Compared to the observed NSD value, the EUR20 shows a slightly better performance than the SWE3 in simulating the spatial variability of seasonal mean precipitation for each season (Fig. S3a, b). The high IOA value (≥ 0.79) between simulated and observed seasonal mean precipitation for each season indicates the good quality of the simulation, although the IOA value is higher for the EUR20 than for the SW3 (Fig. S3a, b). Broadly, it can be inferred that EUR20 performed better in simulating seasonal mean precipitation for each season than the SWE3.

From the above discussion, it is clear that the SWE3 simulated less seasonal mean precipitation than the EUR20 in almost all regions of the IP. In the light of the results, which show a noticeable sensitivity of precipitation associated with the mountain ranges, we perform a detailed evaluation focused on the elevation. To do so, the altitudinal variation (with elevation class of 200 m) of simulated and observed seasonal mean precipitation is calculated for each season using the topography of the simulations. We have only considered the Spain subcontinent in the calculation because the SPREAD dataset is limited to the Spain subcontinent. We have validated the SWE3 with the closest resolution observation only (i.e., SPREAD), and the precipitation and topography of the SWE3 are regridded on a SPREAD grid for the altitudinal variation calculation. The result obtained for each season is shown in Fig. 4a1–d1. To see the added value of the SWE3 over the EUR20, we regridded all the precipitation datasets (both observations and SWE3) on a EUR20 grid, and then we calculated the altitudinal variation of the precipitation for each season using the topography of the EUR20 simulation as shown in Fig. 4a2–d2. The percentage of total grid points covered by each class is also calculated

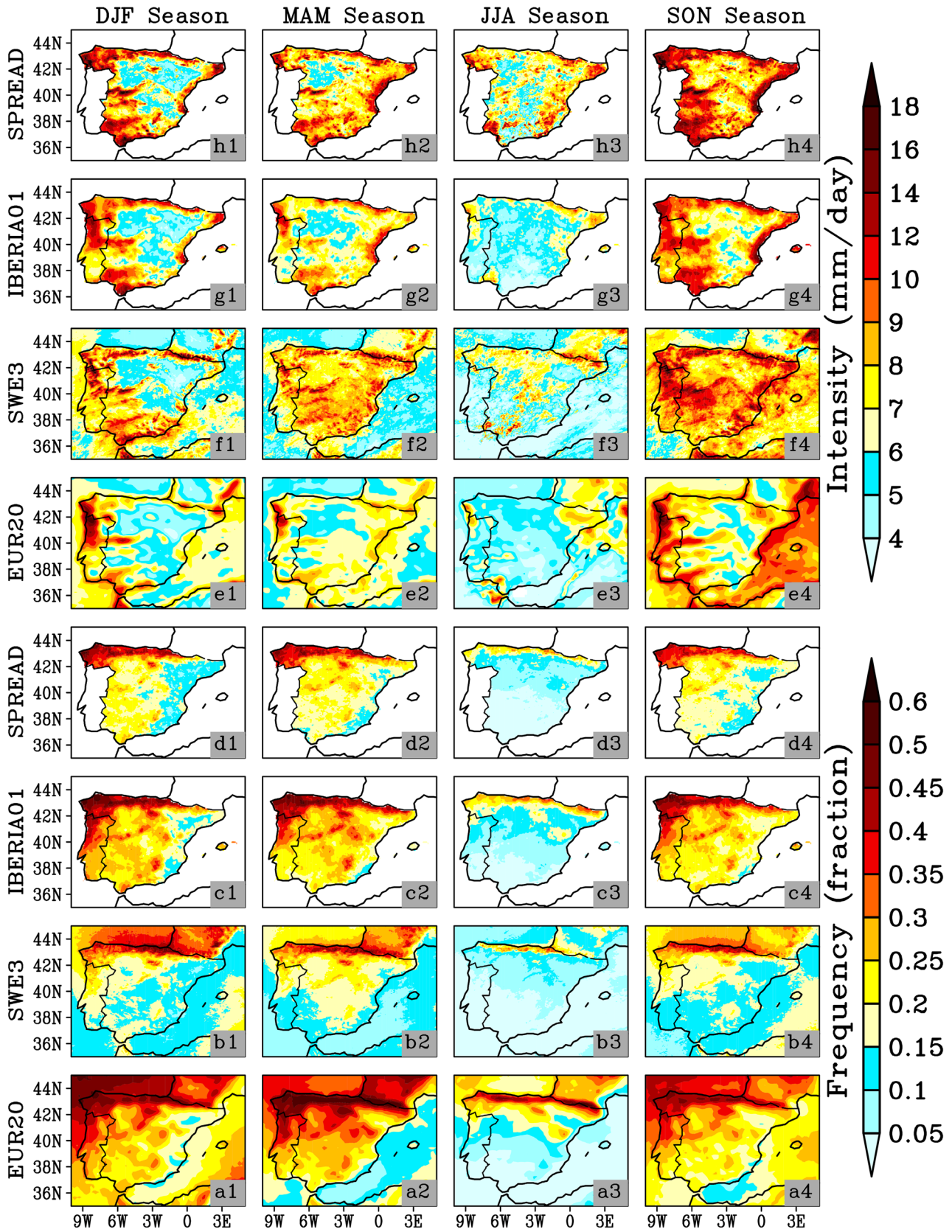
DJF Season
MAM Season
JJA Season
SON Season
SPREAD
IBERIA01
SWE3
EUR20
44N
42N
40N
38N
36N
9W
6W
3W
0
3E
h1
h2
h3
h4
g1
g2
g3
g4
f1
f2
f3
f4
e1
e2
e3
e4
d1
d2
d3
d4
c1
c2
c3
c4
b1
b2
b3
b4
a1
a2
a3
a4
Intensity (mm/day)
18
16
14
12
10
9
8
7
6
5
4
Frequency (fraction)
0.6
0.5
0.45
0.4
0.35
0.3
0.25
0.2
0.15
0.1
0.05

◂**Fig. 7** Frequency and intensity of the precipitation (days where precipitation >= 1 mm) for each season (DJF, MAM, JJA, and SON) from the **a1–a4**, **e1–e4** EUR20, **b1–b4**, **f1–f4** SWE3, **c1–c4**, **g1–g4** IBERIA01, and **d1–d4**, **h1–h4** SPREAD, respectively during 2000–2009. Units of frequency and intensity are in fraction and mm day^{-1}, respectively

on the SPREAD and EUR20 grids and is shown in Fig. 4d1, d2, respectively. The percentage of the actual number of rain gauge stations presented in the IBERIA01 dataset for each class is also calculated and is shown in Fig. 4a2. A topographic map with rain gauge stations is not available for the SPREAD dataset.

On a finer-scale grid, the SWE3 simulation considerably underestimates and overestimates the observed precipitation in areas with elevations up to 1600 m and above 1800 m for the DJF season, respectively (Fig. 4a1). The SWE3 simulated precipitation is much closer to the observed precipitation for the MAM season with some noticeable differences in the low (up to 600 m) and high (above 2600 m) elevation classes (Fig. 4b1). The simulated precipitation is consistent with the observed precipitation in areas with elevations up to 1400 m for the JJA season, and the SWE3 significantly underestimates the observed precipitation in the higher (above 1400 m) elevation classes (Fig. 4c1). For the SON season, the SWE3 simulation significantly underestimates the observed precipitation in almost all elevation classes (Fig. 4d1).

Compared with observations, the EUR20 shows better results than the SWE3 in areas with elevations up to 1200 m for the DJF and SON seasons (Fig. 4a2, d2), so here we can say that the SWE3 deteriorates the results. However, both the simulations are comparable with observations in the higher elevation classes (above 1200 m). For the MAM season, SWE3 deteriorates the results for areas with elevations up to 600 m and is comparable with the observed results in areas with elevations above 600 m (Fig. 4b2). For the JJA season (Fig. 4c2), the SWE3 simulated precipitation is comparable with the observed precipitation (with a slight underestimation) in areas with elevations up to 1200 m, and it worsens the results in the case of the higher elevation classes (above 1200 m). It is also noted that both the observations show almost the same pattern with a slight difference in precipitation magnitude and this difference may be due to the different resolutions of both the observations (Fig. 4a2–d2). Overall, we have not found added value in the simulation of the mean precipitation by the SWE3 over the parent EUR20 in the lowlands areas (area varies with the seasons), although a slight difference is observed in the mean precipitation of both simulations in the mountainous regions, where the observational datasets having considerable uncertainties/inaccuracies in measurements (due to the sparse station density), might strongly limit model evaluation performances. A recent study by Lundquist et al. (2020) reports that the total annual precipitation can be better represented by well-configured high-resolution atmospheric models in mountainous terrains, than with spatial estimates derived from observational products.

3.2 Spatial distribution of mean moisture transport and its convergence

As we observed in the previous section, the SWE3 simulated less seasonal mean precipitation than EUR20 over almost all regions of the IP, so in this section, we have tried to understand the possible dynamical factors responsible for this. In order to understand this, basically, we have calculated the vertically integrated moisture transport (VIMT) and vertically integrated moisture flux convergence (VIMFC). The VIMT and VIMFC have been computed using the moisture budget equation between surface and 300 hPa, since most water vapour exists below 300 hPa. The mathematical form of these equations can be written as:

$$VIMFC = -\nabla.\frac{1}{g}\int_{Ptop}^{Psfc} qVdp = P - E + \frac{\partial w}{\partial t}$$

$$w = \frac{1}{g}\int_{Ptop}^{Psfc} qdp$$

$$VIMT = \frac{1}{g}\int_{Ptop}^{Psfc} qVdp$$

where $\nabla.()$ is the horizontal divergence in pressure coordinates, g is the gravity acceleration, q is the specific humidity, p and $Psfc$ are the surface air pressure, $Ptop$ is the surface air pressure at the top of the atmosphere (300 hPa in our case), $V = (u, v)$ is the horizontal wind vector, P is the precipitation rate, E is the evaporation rate, and w is the total precipitable water and it can be referred to as the storage term. For negligible storage or annual time scales, the term $\partial w/\partial t$ can be neglected (Cullather et al. 2000).

The seasonal mean VIMT patterns from the SWE3 (regridded on a EUR20 gird) and EUR20 simulations for each season are shown in Fig. 5a1–a4, b1–b4, respectively. Similarly, the seasonal mean VIMFC patterns from the SWE3 and EUR20 simulations are shown in Fig. 6a1–a4, b1–b4, respectively. The spatial pattern of VIMT and VIMFC clearly highlights the seasonal differences between the SWE3 and EUR20 simulations in terms of the magnitude and spatial extent of large-scale transport of moisture and its convergence over the IP for all seasons (Figs. 5, 6). The Atlantic Ocean (with the westerly circulation flow) has been found to be one of the major sources of moisture for precipitation over the IP (Gimeno et al.

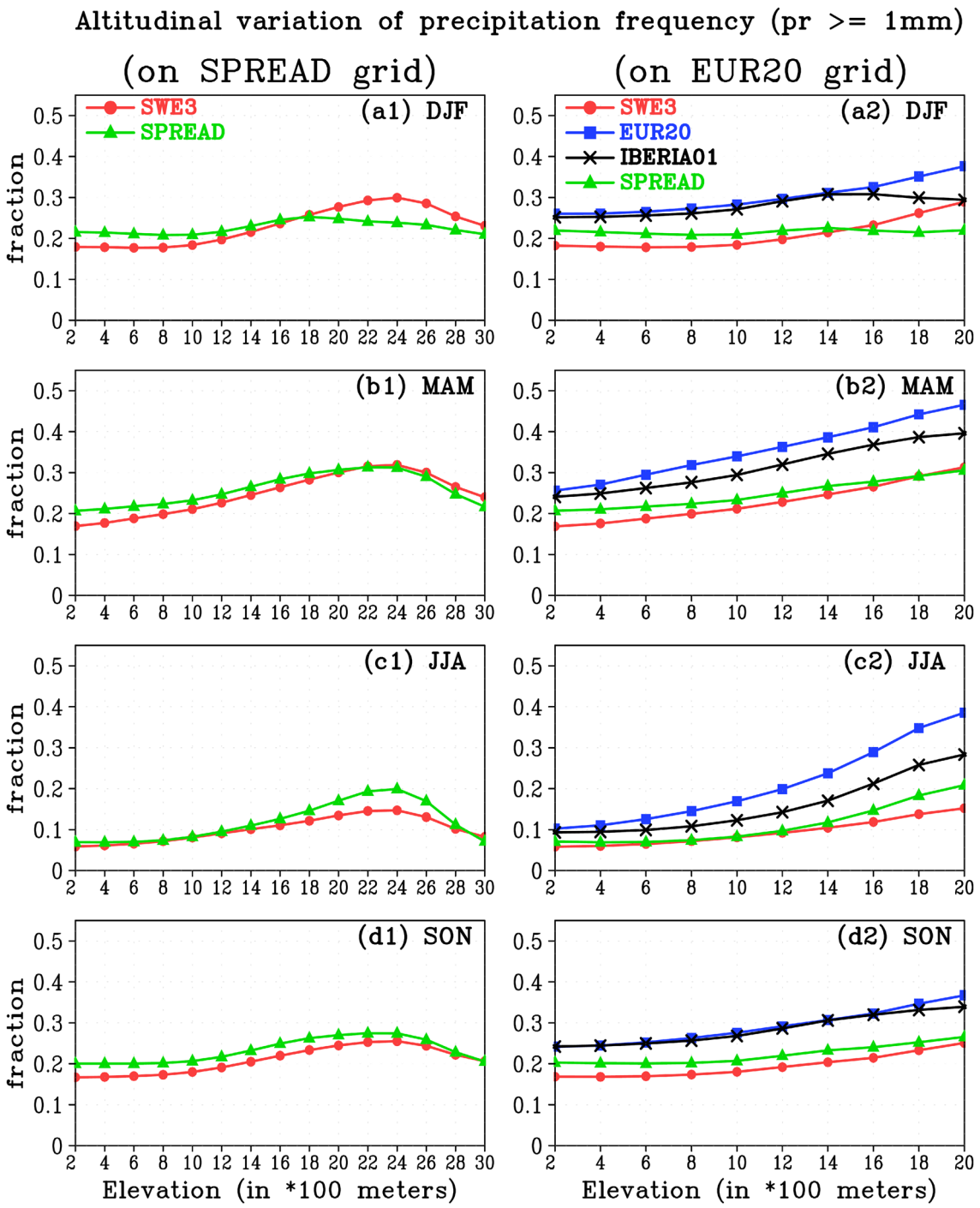

Fig. 8 Altitudinal distribution of precipitation frequency (days where precipitation > = 1 mm) from the SWE3 (red), EUR20 (blue), IBERIA01 (black), and SPREAD (green) over the Iberian Peninsula (IP, over the area of SPREAD observation) on the SPREAD & EUR20 grids for the **a1**, **a2** DJF, **b1**, **b2** MAM, **c1**, **c2** JJA, and **d1**, **d2** SON seasons during 2000–2009. x-axis panels represent the elevation class of 200 m. Units are in fraction

2010, 2012; Şahin et al. 2015). This transport of moisture-laden westerly winds (west–east) from the Atlantic Ocean towards the IP which contributes to the convergence over the IP (resulting into precipitation) can be clearly observed from the EUR20 simulation, and also this pattern is quite persistent for all seasons (Figs. 5b1–b4, 6b1–b4). On the other hand, a slight southeast shift in westerly winds over the Atlantic Ocean has been observed for all seasons except the DJF season, although this signal is more dominant in the JJA season, and this may be associated with

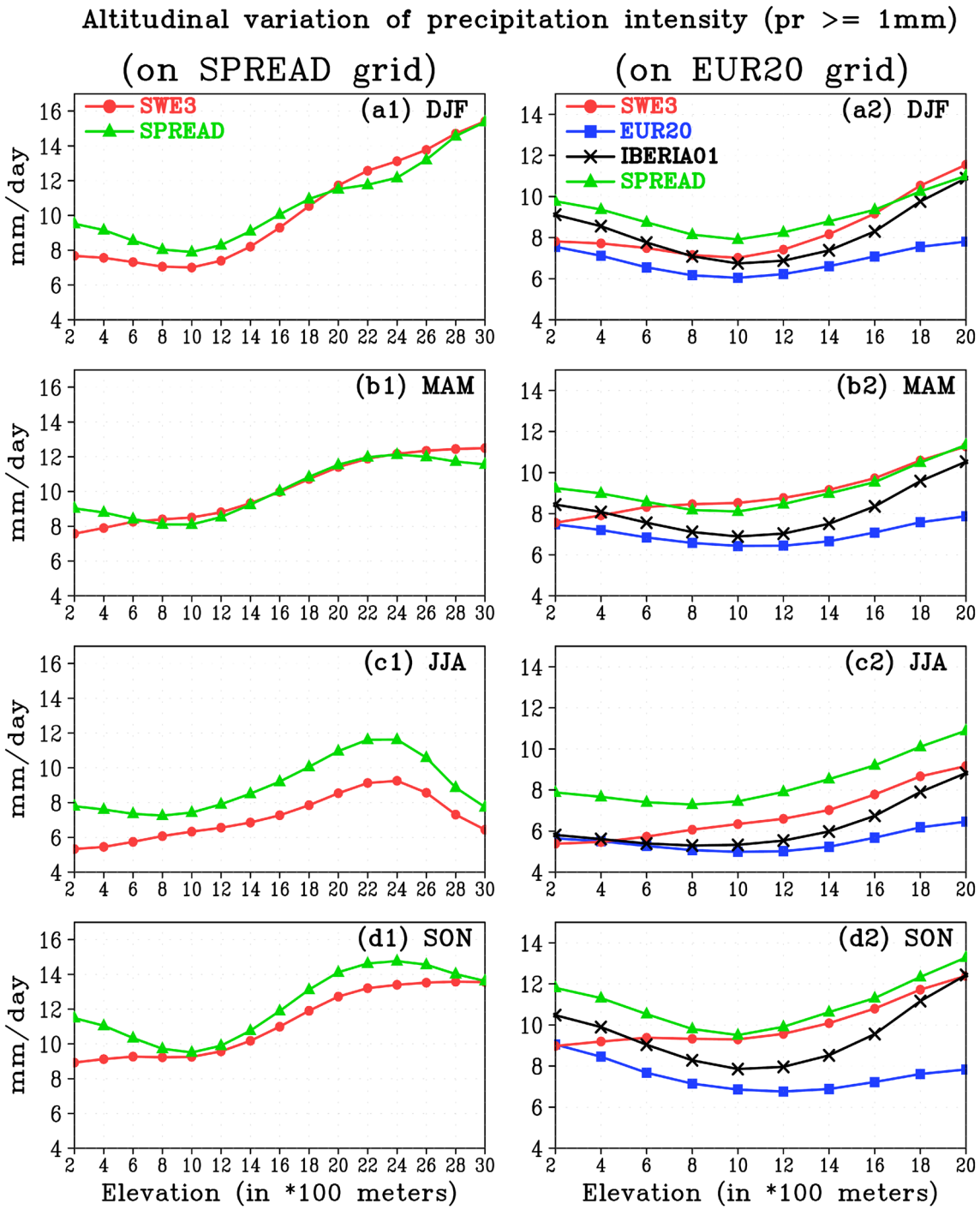

Fig. 9 Altitudinal distribution of precipitation intensity (days where precipitation > = 1 mm) from the SWE3 (red), EUR20 (blue), IBERIA01 (black), and SPREAD (green) over the Iberian Peninsula (IP, over the area of SPREAD observation) on the SPREAD & EUR20 grids for the **a1**, **a2** DJF, **b1**, **b2** MAM, **c1**, **c2** JJA, and **d1**, **d2** SON seasons during 2000–2009. x-axis panels represent the elevation class of 200 m. Units are in mm day^{-1}

the formation of a thermal low-pressure system over the IP that deviates the westerly flow to the southeast direction (Font 1983; Martín et al. 2001; Hoinka and Castro 2003). It is well known that the summer circulation patterns in Iberia are associated to the Iberian thermal low which in some occasions merges with the Saharan thermal low (Hoinka and Castro 2003 and references therein), and the Iberian low is enhanced by the Azorean Anticyclone centered in Mid-Atlantic which forces a strong upwelling signal on the western coast (Romero et al. 1999). The thermal

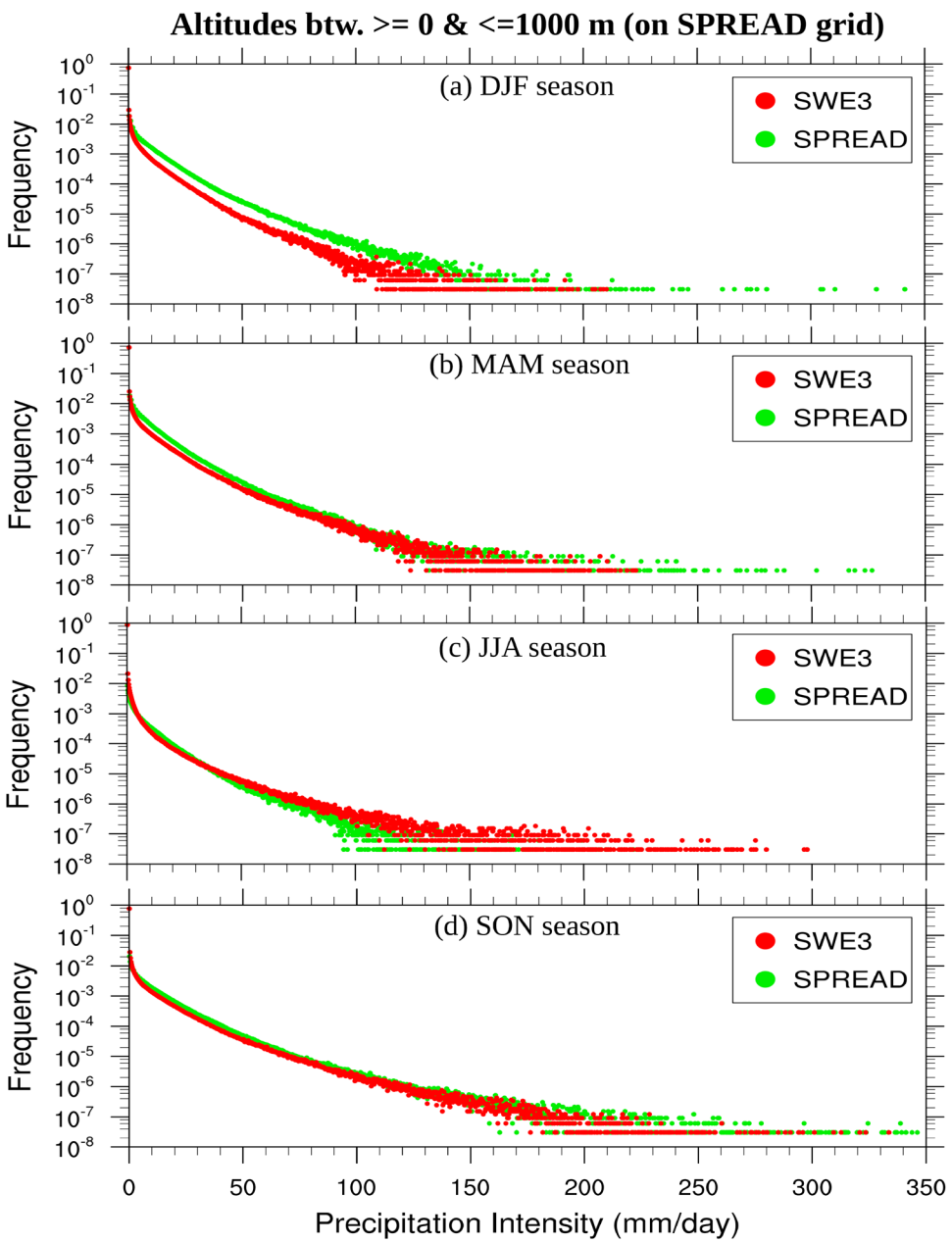

Fig. 10 Probability density function (PDF) of daily mean precipitation (frequency versus intensity) over the Iberian Peninsula (IP, over the area between the altitudes of > = 0 and < = 1000 m of the SPREAD observation) from the SPREAD (green), and SWE3 (red) regridded on the SPREAD grid for **a** DJF, **b** MAM, **c** JJA, and **d** SON seasons during 2000–2009. Units are in mm day^{-1}

low over the IP is more frequent in summer, but it also occurs in spring and autumn (Font 1983). Also in summer, the tropical circulation patterns are known to be associated with southerly and southeasterly warmer wind flows, which dominate over most of the Mediterranean basin, especially in the eastern Mediterranean region (Şahin et al. 2015), and consequently, the southerly blow of winds coming from the southern region towards the northeast direction and its turn to the southeastern direction around the eastern Mediterranean have also been observed, and this resulting pattern is mainly from the northward motion of the inter-tropical convergence zone (ITCZ) and the thermally originated south-Asian monsoon low (Rodwell and Hoskins 1996; Türkeş and Erlat 2006; Şahin et al. 2015), which controls specific humidity over the Mediterranean basin and the land areas around it. However, the eastern Mediterranean circulation has a very minor relevance in the IP.

In the SWE3 simulation, the direction of the wind pattern is significantly different from the EUR20 simulation (Fig. 5). The first difference is that the westerly circulation flow is rotated toward the south in all seasons, although this shift is observed below 40°N in the DJF season (Fig. 5a1–a4). The shift in the wind patterns leads to a decrease in the transport of moisture towards the IP from the Atlantic Ocean, leading to a decrease in precipitation over the IP, especially

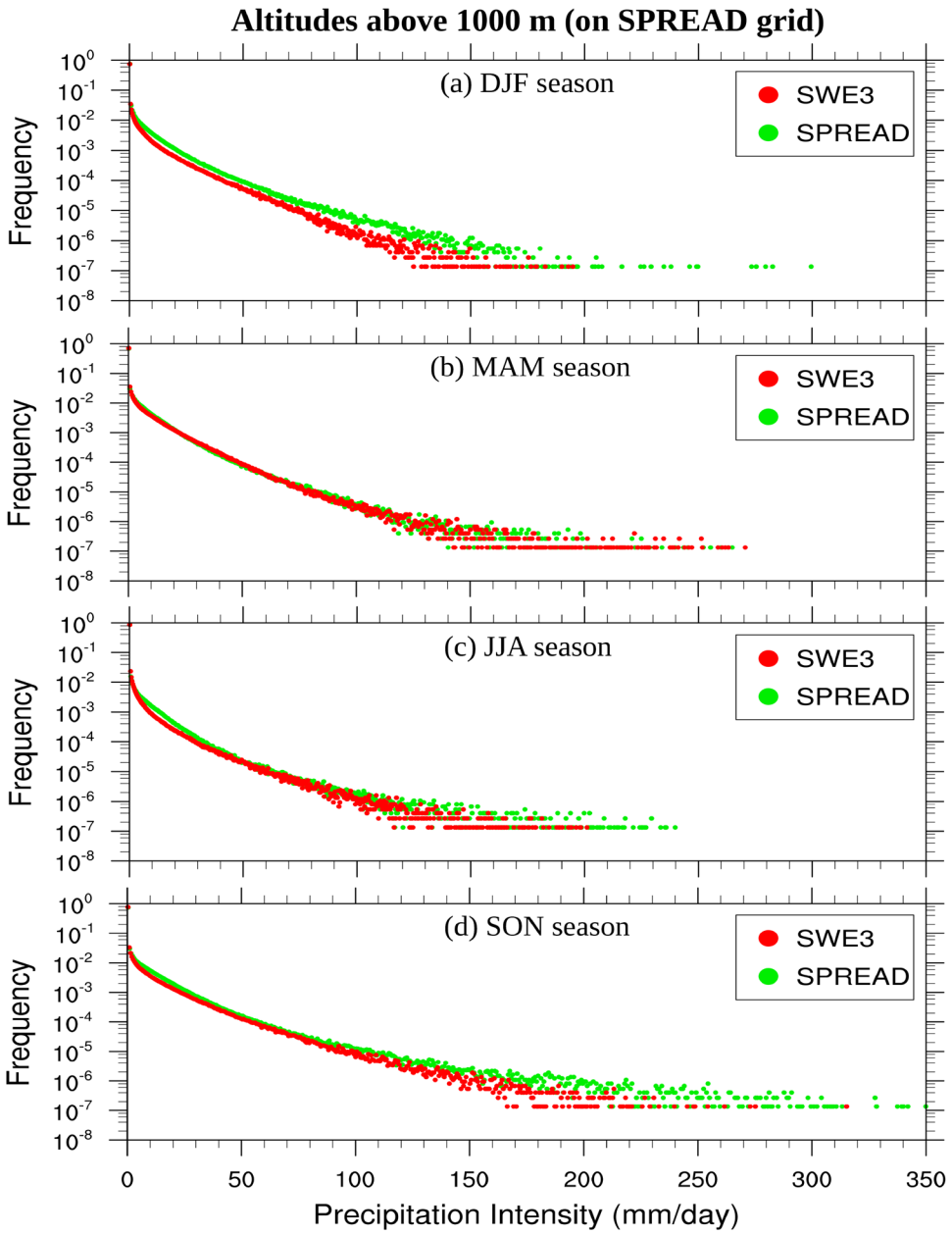

Fig. 11 Probability density function (PDF) of daily mean precipitation (frequency versus intensity) over the Iberian Peninsula (IP, over the area above the altitudes of 1000 m of the SPREAD observation) from the SPREAD (green), and SWE3 (red) regridded on the SPREAD grid for **a** DJF, **b** MAM, **c** JJA, and **d** SON seasons during 2000–2009. Units are in mm day^{-1}

in the western region of the IP, and this is also clear from the VIMFC pattern (Figs. 5a1–a4, 6a1–a4). Apart from the southward shift, a decline in wind strength has also been observed over the western part of the domain, although the wind strength is slightly higher over the southwest boundary in all seasons except DJF season (wind strength is slightly lower in the DJF) and this may be related to the adverse effects of boundary conditions. On the other hand, there is an enhancement of southerly winds (with slightly shifted toward the north) over the Mediterranean basin, and eastern and central regions of the IP have also been observed, which further effectively affect the humidity of these regions as these winds are dry (moisture-free), leading to a decrease in precipitation, and this is also evident from the VIMFC pattern. However, this signal is more prominent in summer and weaker in winter. In the northern region, the north-westerly winds have been observed instead of the westerly flows (west–east), which explains the decrease in precipitation in these regions.

Overall, the large-scale transport of moisture patterns obtained from both simulations explains the differences in precipitation of both simulations. The circulation patterns acquired from the EUR20 simulation are consistent with previous studies (Gimeno et al. 2010; Rios-Entenza et al. 2014; Şahin et al. 2015). As we already know, observations at such high resolutions (3 km) are not available to

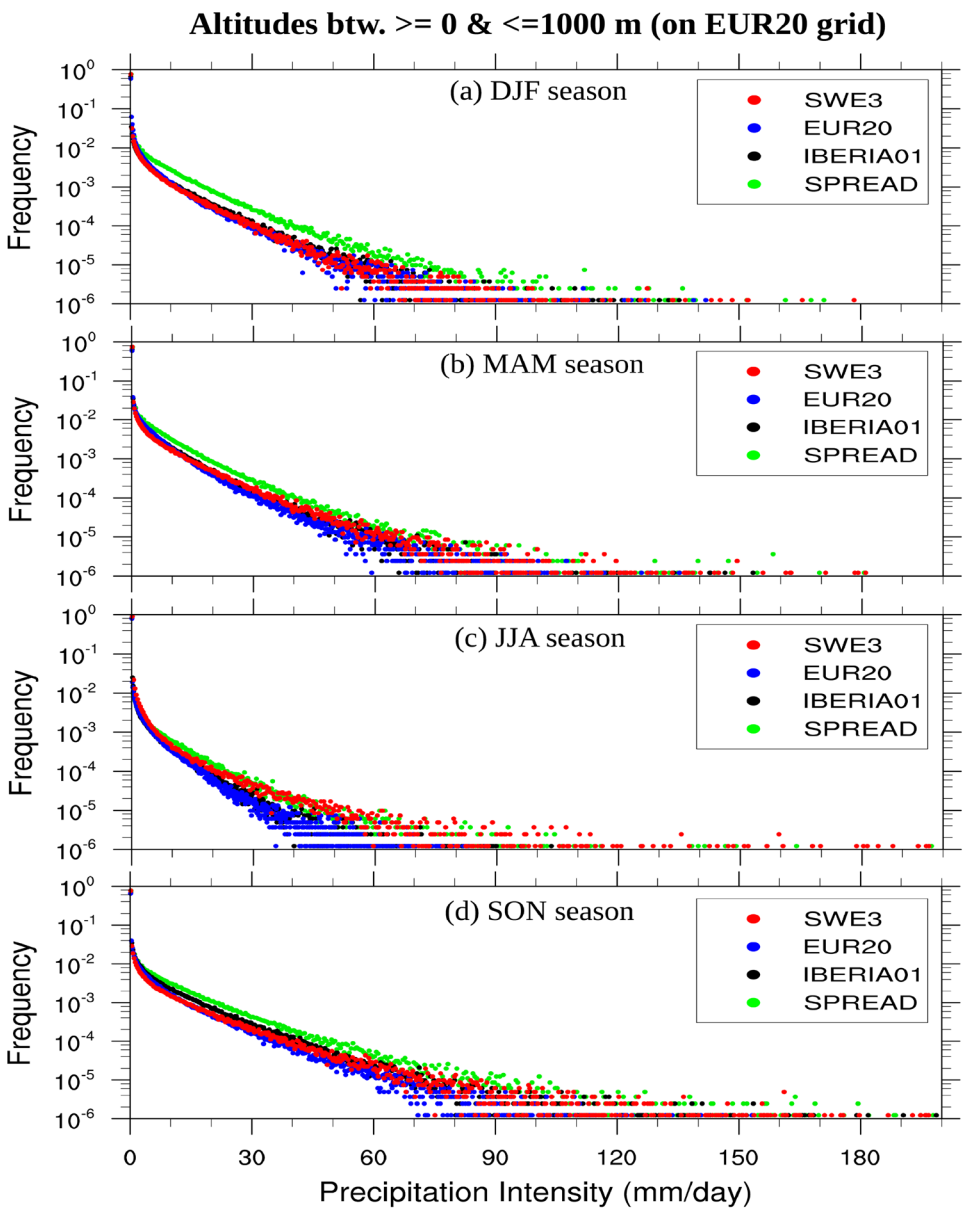

Fig. 12 Probability density function (PDF) of daily mean precipitation (frequency versus intensity) over the Iberian Peninsula (IP, over the area between the altitudes of >=0 and <=1000 m of the SPREAD observation) from the EUR20 (blue), and SWE3 (red), IBERIA01 (black), SPREAD (green) regridded on the EUR20 grid for **a** DJF, **b** MAM, **c** JJA, and **d** SON seasons during 2000–2009. Units are in mm day^{-1}

compare model simulated moisture transport but based on the results of earlier studies (Gimeno et al. 2010; Rios-Entenza et al. 2014; Şahin et al. 2015) we can say that simulated moisture transport by the EUR20 is more logical and reliable. However, local convective processes (terrestrial moisture; precipitation recycling) play a more relevant role in the Iberian precipitation regime during spring and summer, and also the precipitation around Mediterranean coastal regions during the autumn season is mainly associated with frontal activity in the Mediterranean (Bisselink and Dolman 2008; Gimeno et al. 2010; Belo-Pereira et al. 2011; Rios-Entenza et al. 2014). However, a detailed description of these sources (terrestrial moisture sources) is beyond the scope of this paper, and an attempt will be made to explore the terrestrial moisture sources in the modulation of Iberian precipitation in-depth in a separate paper.

We have analyzed the sea level pressure (SLP) of both simulations to explain the change in the circulation patterns of the SWE3. Since we know that the wind is the manifestation of the pressure. The seasonal mean SLP pattern from the SWE3 (regridded on a 20 km gird) and EUR20 simulations for each season is shown in supplementary Figs. S4a1–a4 and S4b1–b4, respectively. We have observed substantial differences in the SLP patterns including the magnitudes (10–15 hPa) of the SWE3 simulation as compared to the EUR20 simulation (supplementary Fig. S4), and this explains the changes in the circulation patterns of the SWE3 (Fig. 5). However, in the summer season, the SLP pattern of the SWE3 is more or

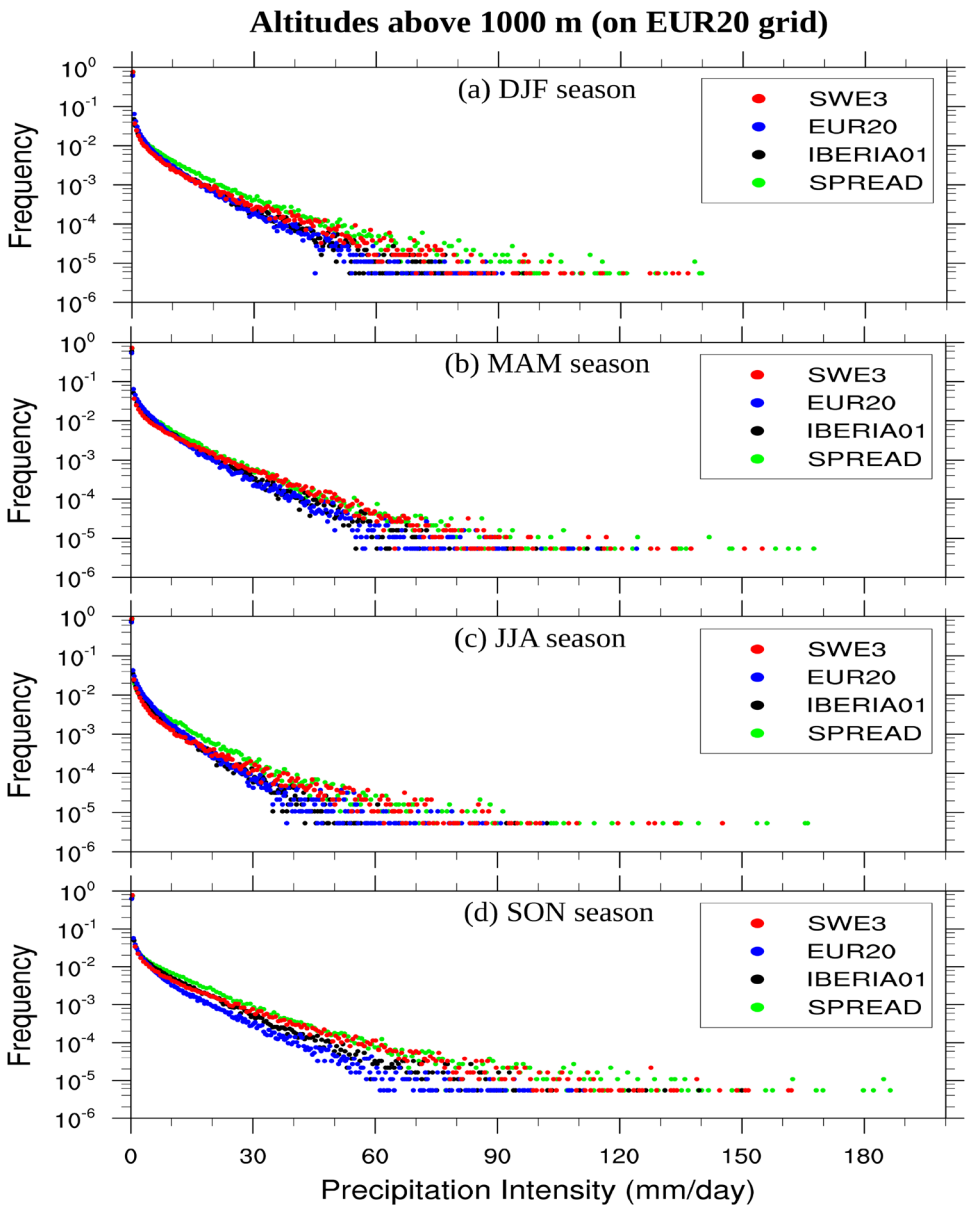

Fig. 13 Probability density function (PDF) of daily mean precipitation (frequency versus intensity) over the Iberian Peninsula (IP, over the area above the altitudes of 1000 m of the SPREAD observation) from the EUR20 (blue), and SWE3 (red), IBERIA01 (black), SPREAD (green) regridded on the EUR20 grid for **a** DJF, **b** MAM, **c** JJA, and **d** SON seasons during 2000–2009. Units are in mm day^{-1}

less similar to the EUR20 SLP pattern with large differences in the magnitude of the SLP (Figs. S4a3–b3). The difference in SLP between the southwest and northwest regions can be clearly observed in the SWE3 (Fig. S4), which explains the deviation/rotation of the westerly flow to the south (as we know that the wind blows from areas of high pressure to areas of low pressure).

The difference in the configuration of SWE3 compared to EUR20 may have "partially" influenced the results of SWE3 in the case of the seasonal mean precipitation. The parametrized representation of convection in EUR20 simulation rather than the explicit treatment in SWE3 simulation may drive the better performance of the EUR20 for seasonal mean precipitation. Berthou et al. (2018) and Ban et al. (2021) highlighted that the convection-permitting climate models (CPCMs) present a decreased number of long-lasting low-intensity precipitation events, which correct and sometimes over-correct the biases of coarse-scale regional climate models (RCMs). This may be a reason for the lower seasonal mean precipitation in SWE3, despite the added values that we note in simulating wet-day frequency and intensity and extreme events later in the manuscript. Also, the Microphysics scheme is different for both simulations which also limits the discussion of the SWE3 results in comparison to the EUR20. However, a further experiment, including these schemes (i.e., cumulus or/and microphysics), is needed to see how much these schemes affect the results of the SWE3.

We speculate that the changes in the behavior of the SLP (and hence the circulation patterns) in the SWE3 simulation could probably attribute to either poor representation

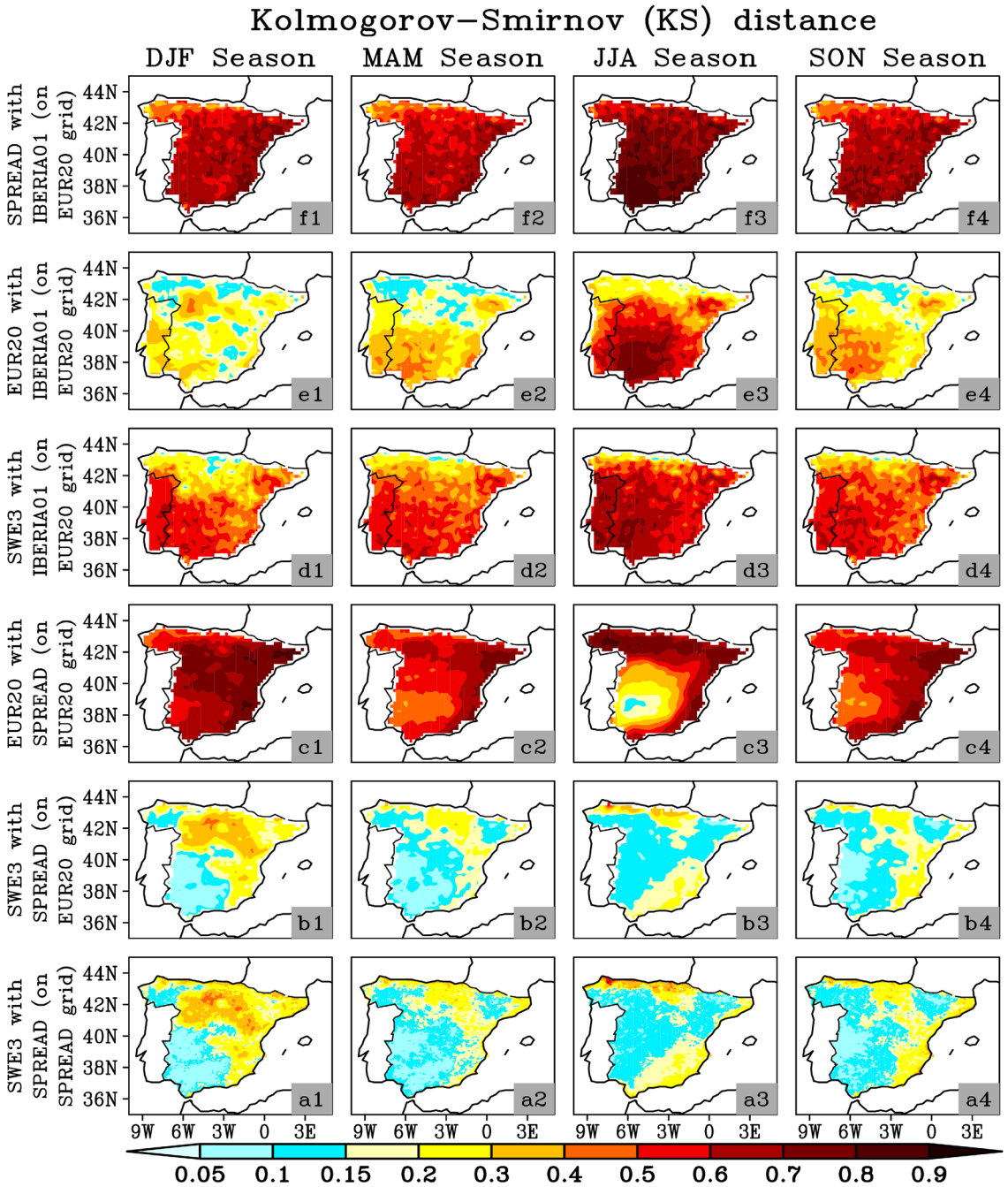

Fig. 14 The Kolmogorov–Smirnov distance between simulated and observed cumulative distribution function (CDF) of daily precipitation for each season during 2000–2009. Results from the **a1**–**a4** SWE3 with SPREAD (on the SPREAD grid), **b1**–**b4** SWE3 with SPREAD (on the EUR20 grid), **c1**–**c4** EUR20 with SPREAD (on the EUR20 grid), **d1**–**d4** SWE3 with IBERIA01 (on the EUR20 grid), **e1**–**e4** EUR20 with IBERIA01 (on the EUR20 grid), and **f1**–**f4** SPREAD with IBERIA01 (on the EUR20 grid)

of lateral boundary conditions (LBCs) or/and poor selection of domain, as the impact of LBC errors represents an important issue in the RCM simulations (Warner et al. 1997; Rinke and Dethloff 2000; Wu et al. 2005; Diaconescu et al. 2007; Køltzow et al. 2008; Diaconescu and Laprise 2013; Brisson et al. 2015; Panosetti et al. 2019; Rocheta et al. 2014, 2020; Ahrens and Leps 2021). Here we mean the errors/biases related to time-dependent large-scale meteorological fields that can flow in the domain through the lateral boundaries. It was found that the choice of domain size and location affects the balance between the boundary and internal model forcings in the simulation

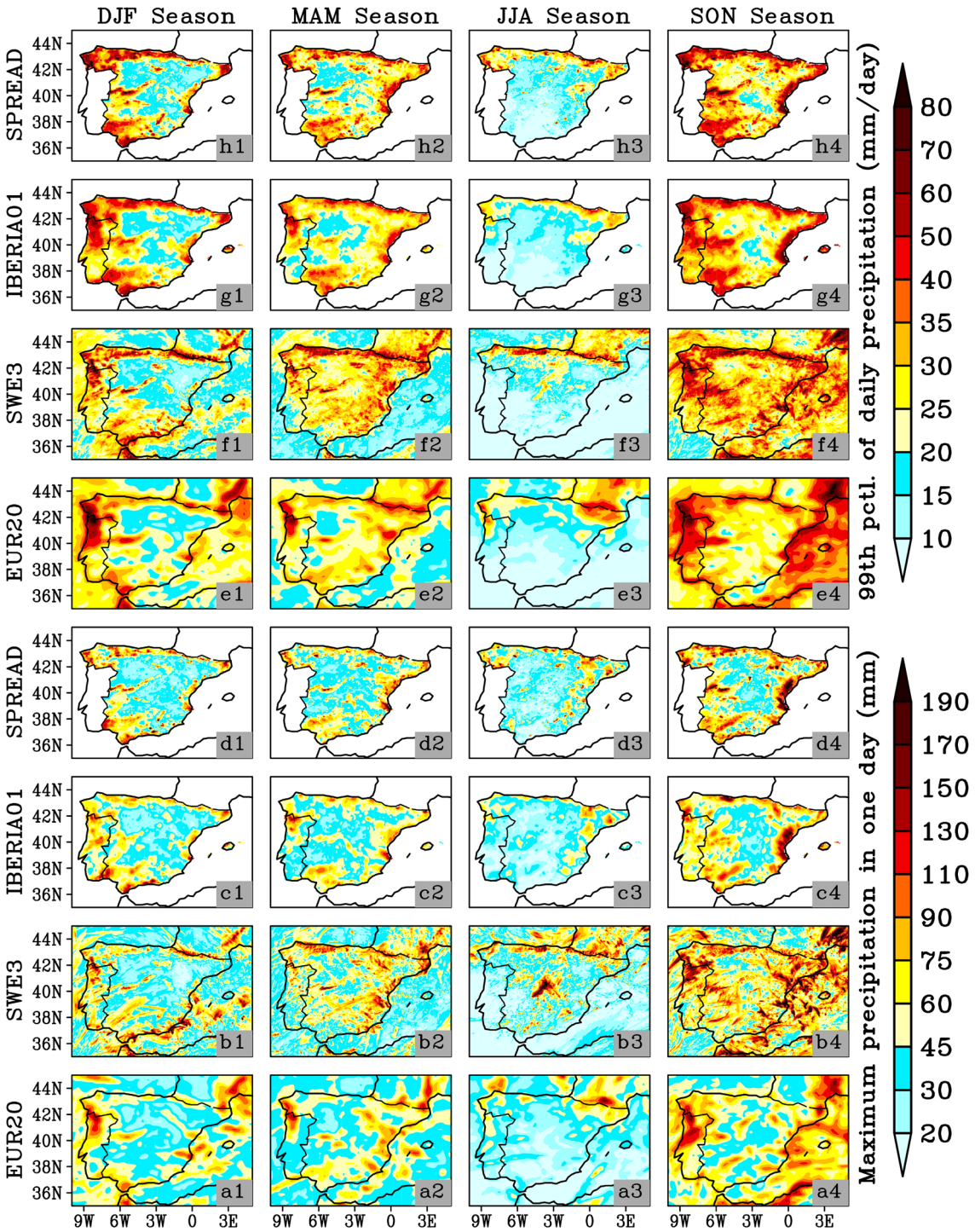

Fig. 15 Maximum one day precipitation amount (Rx1day) and 99th percentile (R99p) of daily mean precipitation for each season (DJF, MAM, JJA, and SON) from the **a1**–**a4**, **e1**–**e4** EUR20, **b1**–**b4**, **f1**–**f4** SWE3, **c1**–**c4**, **g1**–**g4** IBERIA01, and **d1**–**d4**, **h1**–**h4** SPREAD, respectively during 2000–2009. Units of Rx1day and R99p are in mm and mm day^{-1}, respectively

(Anthes et al. 1989; Giorgi and Mearns 1999). The location of boundaries in relation to the regional sources of forcings in a particular climatic region can also affect the regional climate model solution (Rauscher et al. 2006). Seth and Giorgi (1998) also indicated that the lateral boundaries must be placed well outside the region of interest to avoid unrealistic responses to internal forcings. Diaconescu and Laprise (2013) suggested that the RCMs can bring some reduction of errors in large scales when very large domains are used. Several hypothesis-driven modeling experiments

are needed to better understand these results but that would require significant computational resources.

3.3 Spatial distribution of wet-day precipitation frequency and Intensity

The spatial distribution of frequency and intensity of daily mean precipitation (days where the precipitation > = 1 mm) is calculated for each season during 2000–2009 for both simulation and observation and is shown in Fig. 7. Figures 7a1–a4 (7e1–e4), 7b1–b4 (7f1–f4), 7c1–c4 (7g1–g4), and 7d1–d4 (7h1–h4) show the spatial distribution of precipitation frequency (intensity) obtained from the EUR20, SWE3, IBERIA01, and SPREAD, respectively. We have also calculated the altitudinal variation (similar to Fig. 4) of frequency and intensity of wet-day precipitation for each season for quantitative assessment and shown in Figs. 8 and 9, respectively. We have taken only the Spain subcontinent (area of the SPREAD) in the altitudinal variation calculation.

We find that the SWE3 simulation significantly reduced the frequency of the wet-day precipitation not only over the land points of the IP but also over the surrounding oceans for all seasons compared to EUR20 simulation (Figs. 7a1–a4, b1–b4), while it produces more intense wet-day precipitation over the IP subcontinent (Figs. 7e1–e4, f1–f4). In general, convection-permitting models tend to produce less frequent but more intense precipitation intensities compared to coarse resolution models (Berthou et al. 2018; Chan et al. 2020; Ban et al. 2021). On the other hand, the significant differences have also been observed in the magnitude of frequency and intensity of the wet-day precipitation obtained from both observations, as the SPREAD shows less frequent but more intense precipitation than the IBERIA01, and therefore we can say that the frequency and intensity of wet-day precipitation can vary with resolution (Fig. 7). However, the gridded datasets (observations) were not built with the same methodology and with the same number of stations, so the differences in methodology probably play a higher role in the discrepancies between the observational datasets than the resolution. The above results are also evident from Figs. 8 and 9. On the other hand, the spatial structure of the frequency and intensity of wet-day precipitation obtained from the SWE3 (EUR20) shows comparable similarities with respect to the SPREAD (IBERIA01) with some variation in the magnitude of the frequency and intensity at some locations for all seasons, respectively and it may be because of the finer and coarse resolutions of the observed products (Fig. 7). We also observed the significant differences in wet-day precipitation intensity/frequency between the two observations (SPREAD shows less frequent but more intense precipitation than the IBERIA01), and this highlights the uncertainty in the observed dataset (Fig. 7). These results are also clear from Figs. 8 and 9. A detailed comparison of the obtained simulation results with the observed one is discussed below.

The SWE3 simulation substantially underestimates the observed wet-day frequency obtained from the SPREAD in the northwest corner of the IP and slightly underestimates the observed frequency of most other parts of the IP for all seasons (Figs. 7b1–b4, d1–d4), and these results are more pronounced with altitudinal variation (Fig. 8). It can be seen from Fig. 8 that the SWE3 overestimates (underestimates) the observed wet-day frequency of the higher elevation classes for the DJF (JJA) season and is very close to the observed estimates for the remaining two seasons. The SWE3 correctly simulates the observed frequency for the JJA season (in areas with elevations up to 1400 m) and slightly underestimates the observed frequency of most areas of the IP for the rest of the season (Fig. 8). The EUR20 simulation shows almost the same amount of the wet-day frequency as compared to the IBERIA01 for the DJF and SON seasons (Fig. 7a1, a4, c1, c4) with a slight overestimation of the observed frequency of the higher elevation classes (Fig. 8). On the other hand, the EUR20 simulation significantly (slightly) overestimates the observed frequency of the northern (southern) part of the IP for the MAM and JJA seasons (Fig. 7a2–a3, c2–c3) and consequently, the overestimation of the observed frequency by the EUR20 is noted in all elevation classes (Fig. 8). Overall, we noted that the SWE3 results are in good agreement with the closest resolution observation (i.e., SPREAD) whereas the EUR20 results are in line with the IBERIA01, and this highlights the importance of comparing simulations to the dataset with a sufficiently high/comparable resolution to make the comparison fair.

It can be clearly seen that the finer-scale spatial variability with peaks in the mountainous regions of the observed wet-day intensity is relatively well captured by the SWE3 (Fig. 7). The EUR20 simulation significantly underestimates the wet-day intensity in almost all regions of the IP as compared to both observations for all seasons, although maximum differences are observed with the SPREAD (Fig. 7) and these results are more apparent from Fig. 9. The SWE3 simulated more intense wet-day precipitation than the EUR20 in almost all regions of the IP for all seasons, although we did not observe much difference in the precipitation of lowlands areas (in areas with elevations below 400 m for JJA season and 200 m for the rest of the season) between the two simulations for all seasons (Figs. 7, 9). Compared to the IBERIA01, the SWE3 simulation overestimates the wet-day precipitation over most areas of the IP, except that it shows an underestimation of precipitation in some areas of the northwest corner and Mediterranean coasts of southwest and eastern Spain for all the seasons (Fig. 7f1–f4, g1–g4). It is also clear from Fig. 9 that the SWE3 underestimates the observed (IBERIA01) wet-day

precipitation of lowlands areas (in areas with elevations up to 400 m for DJF and SON seasons, and 200 m for the rest of the season) and overestimates the observed precipitation in the remaining regions for all seasons. While compared to the SPREAD, the SWE3 underestimates the wet-day precipitation in almost all regions of the IP for all the seasons, although some overestimation of precipitation is noted in the northern and southern plateau regions of the IP for the MAM season and western parts of the Pyrenees for the DJF season (Fig. 7f1–f4, h1–h4). It can also be seen from Fig. 9 that the SWE3 underestimates the observed (SPREAD) wet-day precipitation of all elevation classes for the JJA and SON seasons, and it is in good agreement with the observed precipitation in areas with elevations above 400 m for the MAM season. Also, the SWE3 underestimates the observed wet-day precipitation in areas with elevations up to 1600 m for the DJF season. Overall, the added value in the SWE3 simulation is found in the reproduction of wet-day intensity as compared to the EUR20 for all seasons. This comparison shows that EUR20 is producing too often too weak precipitation (in line with literature) which turns apparently in a better performance (partially) than SWE3 in terms of mean precipitation, but for the wrong reason.

For the quantitative assessment of simulation performance, the Taylor diagram is produced using the spatial IOA and NSD ratio between observed and simulated frequency and intensity of the wet-day precipitation for each season as shown in supplementary Fig. S5. It is clear from the IOA value that the spatial pattern of the wet-day frequency and intensity of the SPREAD (IBERIA01) are better represented by SWE3 (EUR20) than the EUR20 (SWE3) except for the case of the wet-day intensity of the IBERIA01 for the DJF season where the SWE3 exhibits a higher IOA value than the EUR20 (Fig. S5). It is also noted that the EUR20 overestimates the spatial variability (NSD) of the observed wet-day frequency for all seasons, while the SWE3 underestimates it (Fig. S5a, S5c). The spatial variability of the wet-day frequency of the SPREAD (IBERIA01) is captured quite well by the EUR20 than the SWE3 for the DJF season (DJF-MAM seasons), and the SWE3 shows better skill in simulating the observed spatial variability compared to the EUR20 for the rest of the season (Fig. S5a and S5c). The SWE3 shows better skill in predicting the observed spatial variability of the wet-day intensity than the EUR20 for all the seasons (Figs. S5b and S5d), although SWE3 notably underestimates the observed (SPREAD) spatial variability of the wet-day intensity (Fig. S5b).

In summary, SWE3 simulated less frequent but more intense wet-day precipitation intensities compared to EUR20, and this aspect, in line with the literature (Pichelli et al. 2021; Ban et al. 2021), shows/reflects one of the main benefits in running with an explicit treatment of convection, i.e., a (partial) correction of the too frequent and too weak precipitation usually produced by the convection-parameterized models (EUR20; which can lead a correct mean precipitation for the wrong reason). One thing is clear (with the observational evidence) from the above discussion that the higher resolution datasets have less frequent, but more intense wet-day precipitation intensities compared to the coarse resolution datasets, and also point towards the need of the high-resolution good quality of observational datasets for good estimation.

3.4 Probability distribution of daily mean precipitation

So far, we have observed that the SWE3 simulated less seasonal mean precipitation as compared to the observations (particularly in the western parts of the IP), whereas the seasonal mean precipitation simulated by the EUR20 is closer to the observations. The significant differences have also been noted in simulated and observed wet-day frequency and intensity. However, differences have been observed in the comparative results (also in the precipitation amounts) for lowlands and mountainous regions. Therefore, for a better visualization/comparison of the magnitude of precipitation of the lowlands and mountainous regions in each grid cell, we have classified the total area of Spain's landmass into two elevation classes, which are low (area between the altitudes of ≥ 0 and ≤ 1000 m; which covers about 82% of the total grid points) and high (area above the altitudes of 1000 m; which covers about 18% of the total grid points). We then calculated the PDF of the daily mean precipitation for each category (i.e., low and high) for all seasons on the SPREAD [EUR20] resolution grid as shown in Figs. 10a–d [12a–d] and 11a–d [13a–d], respectively. Please note that we have compared the SWE3 (regridded on a SPREAD grid) results with the closest resolution observation only (i.e., SPREAD) in Figs. 10 and 11. To see the added value of finer-scale simulation (SWE3) over the driving coarse-scale simulation (EUR20), we have regridded all the datasets (both observations and SWE3) before the calculation on a EUR20 grid as shown in Figs. 12 and 13.

In the lowlands regions on a fine-scale grid, the SWE3 simulation underestimates the PDF tail of the SPREAD for all seasons except the JJA season (Fig. 10). However, the underestimation for the DJF season is larger than for the MAM and SON seasons, and the underestimation is very slight for the SON season. The SWE3 simulated tail is very close to the SPREAD in the case of high-intensity precipitation events (≥ 70 and ≤ 220 mm/day) for the MAM and SON seasons (Fig. 10b, d). The SWE3 slightly overestimates and underestimates the observed low (≤ 6 mm/day) and moderate (≥ 8 and ≤ 30 mm/day) intensity precipitation events for the JJA season, respectively (Fig. 10b). On the other hand,

the SWE3 considerably overestimates the occurrence of the observed precipitation events > 50 mm/day for the JJA season (Fig. 10b).

In the mountainous regions on a fine-scale grid, the SWE3 significantly underestimates the observed PDF tail for the DJF season (Fig. 11a). The observed tail of the MAM season is well reproduced by the SWE3 simulation (Fig. 11b). The SWE3 simulated tail is more in line with the observed tail for the JJA season with noticeable underestimations of the low- to moderate-intensity (≥ 6 and ≤ 40 mm/day) and high-intensity (≥ 120 mm/day) observed precipitation events (Fig. 11c). The SWE3 simulated tail is relatively close to the observed tail for the SON season, although significant differences are noted between the tails of the SPREAD and SWE3 in the case of high-intensity (≥ 120 mm/day) precipitation events (Fig. 11d). Since observational rain gauge network stations are very sparse over the highest mountainous areas (e.g., Pyrenees, Baetic, and Cantabrian mountains, etc.), thereby having considerable uncertainties in measurements of the most severe rainfall as well, so any estimation/overestimation of extremes by the model compared with the observed dataset might not be necessarily wrong (but possibly under represented in observations).

The PDFs of the upscaled daily mean precipitation for the lowlands and mountainous regions on a coarse-resolution grid (i.e., EUR20 grid) clearly illustrate the added value of the SWE3 over the EUR20 for all seasons, especially in the occurrence of the moderate- to high-intensity precipitation events (Figs. 12, 13). Significant differences have also been observed in the tails of both observations for all seasons, and this may be due to the different resolution of both datasets as we discussed earlier (Figs. 12, 13).

In the lowlands regions on a upscaled grid, the SWE3 deteriorates the results in the case of low-intensity precipitation events (≤ 15 mm/day) for all seasons except the JJA season, where the clear added value of the SWE3 over the EUR20 has been observed (Fig. 12). The moderate- to high-intensity tail of the SWE3 lies between the tails of both observations for the JJA season, and the SWE3 underestimates the observed SPREAD tail for the rest of the seasons, however, the underestimation is smaller for the MAM and SON seasons compared to the DJF season (Fig. 12). The SWE3 tail is in line with the observed IBERIA01 tail for all seasons, however, the SWE3 slightly underestimates the observed precipitation events of less than 50 mm/day for the SON season and significantly overestimates the observed precipitation events of greater than 25 mm/day for the JJA season (Fig. 12). In the mountainous regions on a upscaled grid, the moderate- to high-intensity tail of the SWE3 lies between the tails of the IBERIA01 and SPREAD for all seasons. However, the SWE3 slightly overestimates and underestimates the occurrence of the moderate- to high-intensity precipitation events (> 30 mm/day) of the IBERIA01 and the SPREAD, respectively (Fig. 13). The EUR20 only simulate events of up to about 140(90):140(125):80(100):150(110) mm/day, while the SWE3 regridded on the EUR20 grid show events reaching about 180(140):180(145):200(155):200(160) mm/day for the DJF: MAM: JJA: SON season in the lowlands (mountainous) regions. Also, the occurrence of intense extreme events simulated by the SWE3 is more in line with the observations. So, a clear benefit of the SWE3 over the EUR20 can be seen in the reproduction of the observed intense extreme events. In summary, we have found significant added value in the simulation of moderate- to high-intensity events of daily precipitation by the SWE3 compared to the driving EUR20, although SWE3 deteriorates the result in the case of low-intensity precipitation events. Also, the maximum added value is seen in the mountainous regions and is in line with earlier studies (Karki et al. 2017; Lind et al. 2020; Ban et al. 2021).

For more quantitative analysis, we have also computed the point-wise K-S distance between the simulated and observed empirical cumulative distribution functions (ECDFs) of daily precipitation for each season during 2000–2009 and the obtained results are shown in Fig. 14. In the first horizontal panel of Fig. 14a1–a4, the SWE3 (regridded on a SPREAD grid) simulation is compared with the closest resolution observation only (i.e., SPREAD). And to explore the added value of the SWE3 over the EUR20, we have regridded all the datasets before the calculation on a EUR20 grid. Figure 14b1–b4 (d1–d4) and c1–c4 (e1–e4) show the statistics obtained from the SWE3 and EUR20 using SPREAD (IBERIA01) observation for each season on a EUR20 grid, respectively. The K-S distance between SPREAD and IBERIA01 on a EUR20 grid is also calculated and is shown in Figs. 14f1-f4 for each season. On a SPREAD grid, the maximum value of KS is around 0.2 over large parts of the IP for all seasons except DJF, where the maximum value of KS reaches around 0.3 (Fig. 14a1–a4) and this can be well explained with PDF tails as we noted the maximum difference in PDF tails of the SWE3 and SPREAD for the DJF season (Figs. 10, 11). On a EUR20 grid, the KS distance is lower for the SWE3 (Fig. 14b1–b4) than the EUR20 (Fig. 14c1–c4) with the SPREAD, whereas with the IBERIA01, the distance is higher for the SWE3 (Fig. 14d1–d4) than the EUR20 (Fig. 14e1–e4) in almost all over the study domain for each season, and it points towards the importance of observed resolution datasets in the comparison of the model simulated outputs. In other words, the added value of SWE3 over the driving EUR20 is obtained with the SPREAD in the representation of KS distance, whereas with the IBERIA01, the SWE3 performance is worse than the EUR20 and it may be due to the coarse resolution of the IBERIA01 datasets. This can also be explained by Fig. 14f1–f4, in which the noticeable difference between the two observations can be clearly seen.

From the above discussion, it is clear that the KS distance of both simulations varies with the observed resolution, and it is likely due to the fact that the tail of the distribution varies with resolution and that can be clearly seen from the PDF plots (Figs. 12, 13). It can also be suggested from the above discussion that the model simulated datasets must be compared with the observational dataset at the same resolution or at the nearest possible one for better estimation.

3.5 Spatio-temporal distribution of heavy/extreme precipitation

To examine the added value of the fine-scale simulation over the driving coarse-scale simulation in the simulation of heavy/extreme precipitation, we have computed the 99th percentile (R99p) of the daily mean precipitation and highest one-day precipitation amount (Rx1day), shown in Fig. 15. Figure 15a1–a4 (e1–e4), b1–b4 (f1–f4), c1–c4 (g1–g4), and d1–d4 (h1–h4) show the spatial distribution of the Rx1day (R99p) for the EUR20, SWE3, IBERIA01, and SPREAD, respectively. The regional to local scales precipitation pattern with clear added value in the SWE3 simulation is observed in the representation of extreme precipitation as compared to the EUR20 for both metrics for all seasons (Fig. 15). It has also been observed that both observations show almost similar precipitation patterns in terms of spatial variability, although some differences in precipitation magnitudes have been noted (Fig. 15). It can be also seen from Fig. 15 that the SWE3 simulation captures the observed precipitation pattern to a great extent, however, there are some biases in the precipitation magnitude at some places, particularly in the southwestern and northwestern regions of Spain and the Mediterranean coasts, but here, we must also take into account the observational uncertainties in the estimation/representation of extreme precipitation events.

For more quantitative assessment, we computed the altitudinal variation (similar to Fig. 4) of the R99p and Rx1day for each season on both resolutions as shown in supplementary Figs. S6 and S7, respectively. It can be seen from the figure that the km-scale simulation shows a clear improvement over the coarse-resolution simulation in the representation of extreme precipitation in almost all the altitudinal classes for all seasons on both grids. However, in the case of R99p, the SWE3 simulated slightly less precipitation than the EUR20 in areas $\leq$ 200 m for MAM & SON seasons, areas $\leq$ 400 m for JJA, and areas $\leq$ 600 m for DJF. On the other hand, differences in the precipitation magnitude of both observations have also been observed in both cases (R99p and Rx1day), although this difference is larger for higher elevation classes (Figs. S6, S7). Furthermore, we noted that the SWE3 simulation underestimates the observed R99p precipitation in lowlands areas and shows a good agreement with observations for the higher elevation classes with slight variation in the magnitude of the precipitation (Fig. S6). In the case of Rx1day, the SWE3 is in agreement with the observed precipitation for all elevation classes with slight variation in the precipitation magnitude (Fig. S7). Overall, these results demonstrate a clear advantage of km-scale simulations in the representation of high-impact precipitation events.

In quantitative terms (Taylor diagram), it is clear from the high IOA value between simulation and observation that the predictive skill of the simulation is greater in the representation of observed extreme precipitation patterns (supplementary Fig. S8). It has also been noted that the IOA value is higher for the R99p than the Rx1day. The SWE3 shows better results than the EUR20 in the representation of the observed (SPREAD) spatial variability of both extreme indices for all seasons, although we have not seen much difference in the IOA value obtained from both simulations for all seasons except JJA, where the EUR20 reflects higher IOA value than the SWE3 (Fig. S8a, S8b). On the other hand, the EUR20 shows a higher IOA value than the SWE3 for the MAM and JJA seasons with the IBERIA01, and we have not seen much difference in the IOA value for the remaining two seasons (Fig. S8c, S8d). In the case of R99p, the SWE3 simulated NSD value is closer to the observed one (IBERIA01) for all seasons except JJA, while in the case of Rx1day, the SWE3 (EUR20) simulated NSD value is closer to the observed one for DJF-SON (MAM-JJA) seasons (Fig. S8c, S8d).

4 Summary and conclusions

The aim of this study is to evaluate the added value of the convection-permitting simulation (3 km, SWE3) compared to the driving coarse-resolution parameterized convection simulation (20 km, EUR20) in the representation of the spatio-temporal pattern of the observed mean and extreme precipitation over the Iberian Peninsula (IP) for all four seasons (i.e., Winter, Spring, Summer, and Autumn) during 2000–2009. Both simulations are performed with the recently developed coupled atmosphere-land RegIPSL regional earth system model in the frame of the EUCP H2020 project and CORDEX. The coarse-scale simulation (20 km grid) is forced by the 6-hourly ERA-Interim (0.75° resolution) initial and lateral boundary conditions (IC-LBCs), while the finer-scale simulation (3 km grid) is driven by the 3-hourly coarse-scale simulated IC-LBCs. The model results are evaluated against two available high-resolution daily gridded observational datasets i.e., SPREAD (5 km grid) and IBERIA01 (10 km grid), and we have also compared the results obtained from the two observations.

No clear benefit/added-value of the convection-permitting simulation has been found in the reproduction of

observed seasonal mean precipitation of the Iberian Peninsula except the spatial variation over hilly peaks compared to coarse-scale simulation for all seasons. The observed spatio-temporal pattern and variability of the seasonal mean precipitation are quantitatively better represented by the coarse-scale simulation than the convection-permitting simulation, and this result is in agreement with previous studies over other areas (Prein et al. 2013, 2016; Warrach-Sagi et al. 2013; Kotlarski et al. 2014) that found a lack of added value of convection-permitting climate simulations in large areal averages and at seasonal scales. However, we have found an added value of the SWE3 compared to the EUR20 in the correct representation of the observed season (including area) of the highest precipitation. The km-scale simulation substantially underestimates the observed seasonal mean precipitation especially over the western parts of the IP compared to the EUR20 simulation which explains that on average over the whole IP, which may be attributed to a change of local dynamics in the kilometer-scale simulation with a weakening and southward shift of the moisture-laden westerly winds approaching from the Atlantic Ocean over the IP. In other words, the shift in the westerlies leads to a decrease in the moisture transport towards the IP from the Atlantic Ocean, leading to a decrease in precipitation. Since we know that the transport of moisture by westerlies from the Atlantic Ocean to the IP is the main moisture supply for the IP precipitation. The differences in wind patterns in the SWE3 are the result of substantial differences in the SLP. Actually, we observed substantial differences in the SLP patterns including the magnitudes (10–15 hPa) of the SWE3 simulation compared to the EUR20 simulation. We speculate that changes in the behavior of the SLP (and hence the circulation patterns) in the SWE3 simulation could probably attribute to the poor representation of lateral boundary conditions (LBCs). We also performed CMIP6 driver SWE3 simulations (as part of the EUCP project) with the exact same model configuration that was used for the ERA-Interim run (this paper is based on the ERA-Interim SWE3 run). The only difference for both simulations was the initial and lateral boundary conditions. Here we would like to mention that in the case of the CMIP6 simulation, we have not observed that much difference in the SLP of the SWE3 compared to the parent simulation (i.e., EUR20), which emphasizes our speculation on the LBC-error propagation. Several hypothesis-driven modeling experiments are needed to better understand these results but that would require significant computational resources/costs. It would be interesting to first see the behavior of the convection-permitting simulation by running the model with the bias correction of lateral boundary conditions.

The clear improvement of kilometric-scale simulation over the driving coarse-scale simulation has been found in the representation of the spatio-temporal distribution of the Kolmogorov–Smirnov (K–S) distance, wet-day precipitation frequency and intensity, and also in the reproduction of the heavy precipitation events for each season. The SWE3 simulated less frequent but more intense wet-day precipitation intensities compared to EUR20, and this aspect, in line with the literature (Pichelli et al. 2021; Ban et al. 2021), shows one of the main benefits in running with an explicit treatment of convection, i.e. a (partial) correction of the too frequent and too weak precipitation usually produced by the convection-parameterized models (EUR20; which at the end results in reasonable mean precipitation but for the wrong reasons). However, SWE3 simulation slightly underestimates the wet-day precipitation frequency and intensity in most areas of the IP as compared to the closest resolution observation (i.e., SPREAD). In the case of the R99p and Rx1day, the significant added value of SWE3 over the driving EUR20 is observed in almost all areas of the IP, and SWE3 is in agreement with the observed estimates with some variation/difference in the magnitude of the precipitation. We observed the significant added value in the simulation of moderate- to high-intensity events of daily precipitation by SWE3 compared to the driving EUR20. Also, the maximum added value has been observed in the mountainous regions of the IP and is in line with previous studies over other areas (Karki et al. 2017; Lind et al. 2020; Ban et al. 2021). Overall, the results demonstrate a clear advantage of km-scale simulation in the representation of high-impact precipitation events. It is likely true that we should use SWE3 simulation to study high-impact weather events because of the intensity of the events. On the other hand, in the mountainous/hilly regions, it is difficult to determine which estimate is correct because observational rain gauge network stations in these areas are very sparse, leading to considerable uncertainty in the measurement of the precipitation. However, we are using two observed datasets at different resolutions which necessarily present differences between them and still with a certain degree of uncertainty related to each one of them, especially over mountainous regions. We can speculate that the SPREAD dataset might be the closest to reality (given its resolution), although supposing it still underestimates the extremes. Given that, we can conclude that any overestimation of the extremes by the model compared with the observed dataset might not be necessarily wrong.

On the other hand, it has also been noted that the spatio-temporal distribution of precipitation for all metrics used varies between the two observational datasets for all seasons, although the difference is weak in the case of the seasonal mean precipitation and large/notable for the wet-day precipitation frequency and intensity and also for the case of the extreme precipitation events, and it may be due to the different resolutions of both observational datasets but also

to other factors such as the number of stations used and the methods of interpolation used in building these datasets. In quantitative terms, SPREAD shows less frequent but more intense wet-day precipitation and more intense extreme precipitation amounts than IBERIA01, and it also highlights the importance of having high-resolution good-quality observed datasets for regional-to-local scale assessments. It has also been noted that the km-scale simulated results are more comparable and closer (in good agreement) with the closest resolution observation (i.e., SPREAD) than IBERIA01 and the opposite is true in the case of coarse-scale simulation, which emphasizes the fact that the model simulated precipitation should be compared with similar or nearly identical resolution observational datasets for better evaluation/estimation and also to make the comparison fair.

These results demonstrate a clear advantage of using a RegIPSL model at the kilometric-scale over the Iberian Peninsula in the simulation for high-impact weather events, consistently with previous studies over other areas, and also point towards the need of the very high-resolution good-quality of observational datasets for the accurate/good evaluation of model-simulated results. It is well documented that the convection-permitting scale models strongly improves the simulation of sub-daily precipitation in many aspects (Hohenegger et al. 2008; Prein et al. 2015; Coppola et al. 2020; Ban et al. 2021; Pichelli et al. 2021; Kendon et al. 2021). This mainly includes the diurnal cycle of mean and extreme precipitation, the frequency-intensity distribution of hourly precipitation, short-time convection in relation with the high and steep mountainous region. However, the absence of sub-daily observed datasets over the Iberian Peninsula did not allow us to examine the added value of the convection-permitting simulation at hourly time scales, but we observed heavier hourly precipitation and a shift in the diurnal cycle. An analysis with particular emphasis on sub-daily precipitation statistics including land surface hydrological processes using the currently available simulations performed by different research groups around Europe (multi-model ensembles) will be presented in a separate paper. The multi-model framework will allow us to estimate the modeling uncertainty for the IP region at the convection-permitting scale, in other words, the multi-model ensembles will allow us to access the quality and reliability of simulations. Also, the multi-model ensembles can provide reliable and accurate high spatial and temporal resolution estimates in this region that can be used in operational applications such as assimilation and/or boundary conditions in numerical weather prediction models and/or analyzed for climate applications. The IP is a very interesting area of study, because a complex topography, various climate regions and different types of precipitation converge within the same environment (Gimeno et al. 2010; Rios-Entenza et al. 2014; Şahin et al. 2015), and the availability of the multi-model ensembles will allow a comprehensive assessment of the potential for improving simulations of not only precipitation characteristics but also other aspects of climate such as land–atmosphere interactions, convective systems, and mountain or urban effects that are impacted by the improved representation of surface heterogeneities.

Supplementary Information The online version contains supplementary material available at https://doi.org/10.1007/s00382-022-06138-y.

Acknowledgements This research was supported/funded by the HORIZON 2020 EUCP (European Climate Prediction system) project (https://www.eucp-project.eu/), under Grant Agreement No. 776613. NKS is thankful to JP and SB for granting the Postdoctoral Fellowship under the H2020 project. NKS gratefully acknowledges Centre national de la recherche scientifique (CNRS) for assistance. Simulations were performed on the French national centre Institut du développement et des ressources en informatique scientifique (IDRIS) with granted access to the high-performance computing (HPC) resources under the allocation A0070100227 made by Grand équipement national de calcul intensif (GENCI). We also thank the Institut Pierre Simon Laplace (IPSL) mésocentre Ensemble de Services Pour la Recherche à l'IPSL (ESPRI) for providing assistance, storage, and computing resources. We thank the two anonymous reviewers for their helpful comments and suggestions that helped us to improve the manuscript.

Author contribution NKS customized the RegIPSL model with the help of JP and RP and performed all the simulations. NKS conceived the study and conducted the analysis and wrote the paper and all other authors provided comments and suggestions for improving the quality of this study.

Funding This work was supported by the HORIZON 2020 EUCP (European Climate Prediction system) project (https://www.eucp-project.eu/), under Grant Agreement No. 776613.

Availability of data and material The datasets used in this work are available on request from the corresponding author.

Code availability The analysis codes are available on request from the corresponding author.

Declarations

Conflict of interest The authors declare that they have no conflict of interest.

References

Ahrens B, Leps N (2021) Sensitivity of convection permitting simulations to lateral boundary conditions in idealised experiments. Earth Space Sci Open Arch ESSOAr. https://doi.org/10.1002/essoar.10506295.1

Anthes RA, Kuo Y-H, Hsie E-Y, Low-Nam S, Bettge TW (1989) Estimation of skill and uncertainty in regional numerical models. Q J R Meteorol Soc 115:763–806. https://doi.org/10.1002/qj.49711548803

Ban N, Schmidli J, Schär C (2014) Evaluation of the convection-resolving regional climate modeling approach in decade-long

simulations. J Geophys Res Atmos 119(13):7889–7907. https://doi.org/10.1002/2014JD021478
Ban N, Caillaud C, Coppola E et al (2021) The first multi-model ensemble of regional climate simulations at kilometer-scale resolution, part I: evaluation of precipitation. Clim Dyn. https://doi.org/10.1007/s00382-021-05708-w
Bechtold P, Chaboureau J-P, Beljaars A, Betts AK, Kohler M, Miller M, Redelsperger J-L (2004) The simulation of the diurnal cycle of convective precipitation over land in a global model. Q J R Meteorol Soc 130:3119–3137. https://doi.org/10.1256/qj.03.103
Belo-Pereira M, Dutra E, Viterbo P (2011) Evaluation of global precipitation data sets over the Iberian Peninsula. J Geophys Res Atmos. https://doi.org/10.1029/2010JD015481
Berthou S, Kendon E, Chan S, Ban N, Leutwyler D, Schar C, Fosser G (2018) Pan-European climate at convection-permitting scale: a model intercomparison study. Clim Dyn 55:35–59. https://doi.org/10.1007/s00382-018-4114-6
Bisselink B, Dolman AJ (2008) Precipitation recycling: moisture sources over Europe using ERA-40 data. J Hydrometeorol 9(5):1073–1083. https://doi.org/10.1175/2008JHM962.1
Brisson E, Demuzere M, van Lipzig NP (2015) Modelling strategies for performing convection-permitting climate simulations. Meteorol Z 25(2):149–163. https://doi.org/10.1127/metz/2015/0598
Brisson E, Van Weverberg K, Demuzere M, Devis A, Saeed S, Stengel M, van Lipzig NP (2016) How well can a convection-permitting climate model reproduce decadal statistics of precipitation, temperature and cloud characteristics? Clim Dyn 47(9–10):3043–3061. https://doi.org/10.1007/s00382-016-3012-z
Brockhaus P, Lüthi D, Schär C (2008) Aspects of the diurnal cycle in a regional climate model. Meteorol Z 17:433–443. https://doi.org/10.1127/0941-2948/2008/0316
Broucke SV, Wouters H, Demuzere M, van Lipzig NP (2019) The influence of convection-permitting regional climate modeling on future projections of extreme precipitation: dependency on topography and timescale. Clim Dyn 52(9):5303–5324. https://doi.org/10.1007/s00382-018-4454-2
Chakravarty IM, Laha RG, Roy J (1967) Handbook of methods of applied statistics, vol I. Wiley, Hoboken, pp 392–394
Chan SC, Kendon EJ, Fowler HJ, Blenkinsop S, Ferro CA, Stephenson DB (2013) Does increasing the spatial resolution of a regional climate model improve the simulated daily precipitation? Clim Dyn 41(5–6):1475–1495. https://doi.org/10.1007/s00382-012-1568-9
Chan SC, Kendon EJ, Berthou S, Fosser G, Lewis E, Fowler HJ (2020) Europe-wide precipitation projections at convection permitting scale with the Unified Model. Clim Dyn 55:409–428. https://doi.org/10.1007/s00382-020-05192-8
Chang W, Wang J, Marohnic J, Kotamarthi VR, Moyer EJ (2020) Diagnosing added value of convection-permitting regional models using precipitation event identification and tracking. Clim Dyn 55(1):175–192. https://doi.org/10.1007/s00382-018-4294-0
Coppola E, Sobolowski S, Pichelli E, Raffaele F, Ahrens B, Anders I, Ban N, Bastin S, Belda M, Belusic D et al (2020) A first-of-its-kind multi-model convection permitting ensemble for investigating convective phenomena over Europe and the Mediterranean. Clim Dyn 55:3–34. https://doi.org/10.1007/s00382-018-4521-8
Cullather RI, Bromwich DH, Serreze MC (2000) The atmospheric hydrologic cycle over the Arctic basin from reanalysis. Part I: comparison with observation and previous studies. J Clim 13(923):937. https://doi.org/10.1175/1520-0442(2000)013%3C0923:TAHCOT%3E2.0.CO;2
Dee DP, Uppala SM, Simmons AJ et al (2011) The ERA-Interim reanalysis: configuration and performance of the data assimilation system. Q J R Meteorol Soc 137:535–597. https://doi.org/10.1002/qj.828
Déqué M, Rowell MP, Lüthi D, Giorgi F, Christensen JH, Rockel B, Jacob D, Kjellström E, de Castro M, van den Hurk B (2007) An intercomparison of regional climate simulations for Europe: assessing uncertainties in model projections. Clim Change 81:53–70. https://doi.org/10.1007/s10584-006-9228-x
Diaconescu EP, Laprise R (2013) Can added value be expected in RCM-simulated large scales? Clim Dyn 41(7):1769–1800. https://doi.org/10.1007/s00382-012-1649-9
Diaconescu EP, Laprise R, Sushama L (2007) The impact of lateral boundary data errors on the simulated climate of a nested regional climate model. Clim Dyn 28(4):333–350. https://doi.org/10.1007/s00382-006-0189-6
Fita L, Polcher J, Giannaros TM, Lorenz T, Milovac J, Sofiadis G, Katragkou E, Bastin S (2019) CORDEX-WRF v1.3: development of a module for the Weather Research and Forecasting (WRF) model to support the CORDEX community. Geosci Model Dev 12(3):1029–1066. https://doi.org/10.5194/gmd-12-1029-2019
Font I (1983) Climatología de España y Portugal (Climate of Spain and Portugal). Inst Nacional de Meteorología. Ministerio de Transportes y Comunicaciones de Madrid, p 296
Fosser G, Khodayar S, Berg P (2015) Benefit of convection permitting climate model simulations in the representation of convective precipitation. Clim Dyn 44:45–60. https://doi.org/10.1007/s00382-014-2242-1
Frei C, Christensen JH, Dèquè M, Jacob D, Jones RG, Vidale PL (2003) Daily precipitation statistics in regional climate models: evaluation and intercomparison for the European Alps. J Geophys Res Atmos 108:4124. https://doi.org/10.1029/2002JD002287
Fumière Q, Déqué M, Nuissier O, Somot S, Alias A, Caillaud C, Laurantin O, Seity Y (2019) Extreme rainfall in Mediterranean France during the fall: added-value of the CNRM-AROME Convection-Permitting Regional Climate Model. Clim Dyn 55:77–91. https://doi.org/10.1007/s00382-019-04898-8
Gimeno L, Nieto R, Trigo RM, Vicente-Serrano SM, López-Moreno JI (2010) Where does the Iberian Peninsula moisture come from? An answer based on a Lagrangian approach. J Hydrometeorol 11:421–436. https://doi.org/10.1175/2009JHM1182.1
Gimeno L, Stohl A, Trigo RM, Dominguez F, Yoshimura K, Yu L, Drumond A, Durán-Quesada AM, Nieto R (2012) Oceanic and terrestrial sources of continental precipitation. Rev Geophys 50(4):RG4003. https://doi.org/10.1029/2012RG000389
Giorgi F, Mearns LO (1999) Introduction to special section: regional climate modeling revisited. J Geophys Res Atmos 104:6335–6352. https://doi.org/10.1029/98JD02072
Helsen S, van Lipzig NP, Demuzere M, Broucke SV, Caluwaerts S, De Cruz L, De Troch R, Hamdi R, Termonia P, Van Schaeybroeck B, Wouters H (2020) Consistent scale-dependency of future increases in hourly extreme precipitation in two convection-permitting climate models. Clim Dyn 54(3):1267–1280. https://doi.org/10.1007/s00382-019-05056-w
Herrera S, Gutiérrez JM, Ancell R, Pons MR, Frías MD, Fernandez J (2010) Development and analysis of a 50-year high-resolution daily gridded precipitation dataset over Spain (Spain02). Int J Climatol 32:74–85. https://doi.org/10.1002/joc.2256
Herrera S, Cardoso RM, Soares PM, Espírito-Santo F, Viterbo P, Gutiérrez JM (2019) Iberia01: a new gridded dataset of daily precipitation and temperatures over Iberia. Earth Syst Sci Data 11:1947–1956. https://doi.org/10.5194/essd-11-1947-2019
Hohenegger C, Brockhaus P, Schär C (2008) Towards climate simulations at cloud-resolving scales. Meteorol Z 17(4):383–394. https://doi.org/10.1127/0941-2948/2008/0303
Hoinka KP, Castro MD (2003) The Iberian peninsula thermal low. Q J R Meteorol Soc 129(590):1491–1511. https://doi.org/10.1256/qj.01.189
Isotta F, Frei C, Weilguni V, Tadić MP, Lasségues P, Rudolf B, Pavan V, Cacciamani C, Antolini G, Ratto SM, Munari M, Micheletti

S, Bonati V, Lussana C, Ronchi C, Panettieri E, Marigo G, Vertačnik G (2014) The climate of daily precipitation in the Alps: development and analysis of a high-resolution grid dataset from pan-Alpine rain-gauge data. Int J Climatol 34(5):1657–1675. https://doi.org/10.1002/joc.3794

Jacob D, Petersen J, Eggert B et al (2014) EURP-CORDEX: new high-resolution climate change projections for European impact research. Reg Environ Change 14(2):563–578. https://doi.org/10.1007/s10113-013-0499-2

Karki R, Gerlitz L, Schickhoff U, Scholten T, Böhner J (2017) Quantifying the added value of convection-permitting climate simulations in complex terrain: a systematic evaluation of WRF over the Himalayas. Earth Syst Dyn 8:507–528. https://doi.org/10.5194/esd-8-507-2017

Karl TR, Nicholls N, Ghazi A (1999) CLIVAR/GCOS/WMO workshop on indices and indicators for climate extremes. Clim Change 42:3–7. https://doi.org/10.1023/A:1005491526870

Kendon EJ, Roberts NM, Senior CA, Roberts MJ (2012) Realism of rainfall in a very high-resolution regional climate model. J Clim 25(17):5791–5806. https://doi.org/10.1175/JCLI-D-11-00562.1

Kendon EJ, Roberts NM, Fowler HJ, Roberts MJ, Chan SC, Senior CA (2014) Heavier summer downpours with climate change revealed by weather forecast resolution model. Nat Clim Change 4(7):570–576. https://doi.org/10.1038/nclimate2258

Kendon EJ, Ban N, Roberts NM, Fowler HJ, Roberts MJ, Chan SC, Evans JP, Fosser G, Wilkinson JM (2017) Do convection-permitting regional climate models improve projections of future precipitation change? Bull Am Meteorol Soc 98(1):79–93. https://doi.org/10.1175/BAMS-D-15-0004.1

Kendon EJ, Stratton RA, Tucker S, Marsham JH, Berthou S, Rowell DP, Senior CA (2019) enhanced future changes in wet and dry extremes over Africa at convection-permitting scale. Nat Commun 10:1794. https://doi.org/10.1038/s41467-019-09776-9

Kendon EJ, Prein AF, Senior CA, Stirling A (2021) Challenges and outlook for convection-permitting climate modelling. Philos Trans R Soc A 379:20190547. https://doi.org/10.1098/rsta.2019.0547

Knist S, Goergen K, Simmer C (2020) Evaluation and projected changes of precipitation statistics in convection-permitting WRF climate simulations over Central Europe. Clim Dyn 55:325–341. https://doi.org/10.1007/s00382-018-4147-x

Køltzow M, Iversen T, Haugen JE (2008) Extended Big-Brother experiments: the role of lateral boundary data quality and size of integration domain in regional climate modelling. Tellus A 60(3):398–410. https://doi.org/10.1111/j.1600-0870.2007.00309.x

Kotlarski S, Keuler K, Christensen OB, Colette A, Déqué M, Gobiet A, Goergen K, Jacob D, Lüthi D, van Meijgaard E, Nikulin G, Schär C, Teichmann C, Vautard R, Warrach-Sagi K, Wulfmeyer V (2014) Regional climate modeling on european scales: a joint standard evaluation of the EURO-CORDEX RCM ensemble. Geosci Model Dev 7(4):1297–1333. https://doi.org/10.5194/gmd-7-1297-2014

Kouadio K, Bastin S, Konare A, Ajayi VO (2020) Does convection-permitting simulate better rainfall distribution and extreme over Guinean coast and surroundings? Clim Dyn 55(1):153–174. https://doi.org/10.1007/s00382-018-4308-y

Krinner G, Viovy N, de Noblet-Ducoudré N, Ogée J, Polcher J, Friedlingstein P, Ciais P, Sitch S, Prentice IC (2005) A dynamic global vegetation model for studies of the coupled atmosphere-biosphere system. Glob Biogeochem Cycles 19(1):GB1015. https://doi.org/10.1029/2003GB002199

Leutwyler D, Lüthi D, Ban N, Fuhrer O, Schär C (2017) Evaluation of the convection-resolving climate modeling approach on continental scales. J Geophys Res Atmos 122(10):5237–5258. https://doi.org/10.1002/2016JD026013

Li P, Guo Z, Furtado K, Chen H, Li J, Milton S, Field PR, Zhou T (2019) Prediction of heavy precipitation in the eastern China flooding events of 2016: added value of convection-permitting simulations. Q J R Meteorol Soc 145(724):3300–3319. https://doi.org/10.1002/qj.3621

Li P, Furtado K, Zhou T, Chen H, Li J (2021) Convection-permitting modelling improves simulated precipitation over the central and eastern Tibetan Plateau. Q J R Meteorol Soc 147(734):341–362. https://doi.org/10.1002/qj.3921

Lind P, Lindstedt D, Kjellström E, Jones C (2016) Spatial and temporal characteristics of summer precipitation over central Europe in a suite of high-resolution climate models. J Clim 29(10):3501–3518. https://doi.org/10.1007/s00382-018-4114-6

Lind P, Belušić D, Christensen OB, Dobler A, Kjellström E, Landgren O, Lindstedt D, Matte D, Pedersen RA, Toivonen E, Wang F (2020) Benefits and added value of convection-permitting climate modeling over fenno-scandinavia. Clim Dyn 55(7):1893–1912. https://doi.org/10.1007/s00382-020-05359-3

Liu C, Ikeda K, Rasmussen R, Barlage M, Newman AJ, Prein AF, Chen F, Chen L, Clark M, Dai A, Dudhia J, Eidhammer T, Gochis D, Gutmann E, Kurkute S, Li Y, Thompson G, Yates D (2017) Continental-scale convection-permitting modeling of the current and future climate of North America. Clim Dyn 49(1):71–95. https://doi.org/10.1007/s00382-016-3327-9

Lundquist J, Hughes M, Gutmann E, Kapnick S (2020) Our skill in modeling mountain rain and snow is bypassing the skill of our observational networks. Bull Am Meteorol Soc 100(12):2473–2490. https://doi.org/10.1175/BAMS-D-19-0001.1

Madec G, Delecluse P, Imbard M, Levy C (1998) Opa 8 ocean general circulation model—reference manual. Tech rep LODYC/IPSL Note 11

Martín F, Crespí SN, Palacios M (2001) Simulations of mesoscale circulations in the center of the Iberian Peninsula for thermal low pressure conditions. Part I: evaluation of the topography vorticity-mode mesoscale model. J Appl Meteorol 40(5):880–904. https://doi.org/10.1175/1520-0450(2001)040%3C0880:SOMCIT%3E2.0.CO;2

Meredith E, Maraun D, Semenov V, Park W (2015) Evidence for added value of convection permitting models for studying changes in extreme precipitation. J Geophys Res Atmos 120:12500–12513. https://doi.org/10.1002/2015JD024238

Muñoz-Diaz D, Rodrigo FS (2004) Spatio-temporal patterns of seasonal rainfall in Spain (1912–2000) using cluster and principal component analysis: comparison. Ann Geophys 22:1435–1448. https://doi.org/10.5194/angeo-22-1435-2004

Panosetti D, Schlemmer L, Schär C (2019) Bulk and structural convergence at convection-resolving scales in real-case simulations of summertime moist convection over land. Q J R Meteorol Soc 145(721):1427–1443. https://doi.org/10.1002/qj.3502

Peterson TC (2005) Climate change indices. WMO Bull 54(2):83–86

Pichelli E, Coppola E, Sobolowski S et al (2021) The first multi-model ensemble of regional climate simulations at kilometer-scale resolution part 2: historical and future simulations of precipitation. Clim Dyn 56(11):3581–3602. https://doi.org/10.1007/s00382-021-05657-4

Prein AF, Gobiet A (2017) Impacts of uncertainties in european gridded precipitation observations on regional climate analysis. Int J Climatol 37(1):305–327. https://doi.org/10.1002/joc.4706

Prein A, Gobiet A, Suklitsch M, Truhetz H, Awan N, Keuler K, Georgievski G (2013) Added value of convection permitting seasonal simulations. Clim Dyn 41:2655–2677. https://doi.org/10.1007/s00382-013-1744-6

Prein AF, Langhans W, Fosser G, Ferrone A, Ban N, Goergen K, Keller M, Tölle M, Gutjahr O, Feser F, Brisson E, Kollet S, Schmidli J, van Lipzig NPM, Leung R (2015) A review on regional convection-permitting climate modeling: demonstrations, prospects, and challenges. Rev Geophys 53(2):323–361. https://doi.org/10.1002/2014RG000475

Prein AF, Gobiet A, Truhetz H, Keuler K, Goergen K, Teichmann C, Fox Maule C, van Meijgaard E, Déqué M, Nikulin G, Vautard

R, Colette A, Kjellström E, Jacob D (2016) Precipitation in the EURO-CORDEX 0.11° and 0.44° simulations: high resolution, high benefits? Clim Dyn 46(1–2):383–412. https://doi.org/10.1007/s00382-015-2589-y

Randall DA, Wood RA, Bony S, Colman R, Fichefet T, Fyfe J, Kattsov J, Pitman A, Shukla J, Srinivasan J, Stouffer RJ, Sumi A, Taylor KE (2007) Cilmate models and their evaluation. In: Solomon S, Qin D, Manning M, Chen Z, Marquis M, Averyt KB, Tignor M, Miller HL (eds) Climate change 2007: the physical science basis Contribution of working group I to the fourth assessment report of the intergovernmental panel on climate change. Cambridge University Press, Cambridge

Rasmussen KL, Prein AF, Rasmussen RM, Ikeda K, Liu C (2020) Changes in the convective population and thermodynamic environments in convection-permitting regional climate simulations over the United States. Clim Dyn 55(1):383–408. https://doi.org/10.1007/s00382-017-4000-7

Rauscher SA, Seth A, Qian JH, Camargo SJ (2006) Domain choice in an experimental nested modeling prediction system for South America. Theor Appl Climatol 86:229–246. https://doi.org/10.1007/s00704-006-0206-z

Rinke A, Dethloff K (2000) On the sensitivity of a regional Arctic climate model to initial and boundary conditions. Clim Res 14:101–113. https://doi.org/10.3354/cr014101

Rios-Entenza A, Soares PM, Trigo RM, Cardoso RM, Miguez-Macho G (2014) Moisture recycling in the Iberian Peninsula from a regional climate simulation: spatiotemporal analysis and impact on the precipitation regime. J Geophys Res Atmos 119(10):5895–5912. https://doi.org/10.1002/2013JD021274

Rocheta E, Evans JP, Sharma A (2014) Assessing atmospheric bias correction for dynamical consistency using potential vorticity. Environ Res Lett 9(12):124010. https://doi.org/10.1088/1748-9326/9/12/124010

Rocheta E, Evans JP, Sharma A (2020) Correcting lateral boundary biases in regional climate modeling-the effect of the relaxation zone. Clim Dyn 55(9):2511–2521. https://doi.org/10.1007/s00382-020-05393-1

Rodwell MJ, Hoskins B (1996) Monsoons and the dynamics of deserts. Q J R Meteorol Soc 122:1385–1404. https://doi.org/10.1002/qj.49712253408

Romero R, Sumner G, Ramis C, Genovés A (1999) A classification of the atmospheric circulation patterns producing significant daily rainfall in the Spanish Mediterranean area. Int J Climatol 19(7):765–785

Ruti PM, Somot S, Giorgi F et al (2015) MED-CORDEX initiative for Mediterranean climate studies. Bull Am Meteorol Soc 97(7):1187–1208. https://doi.org/10.1175/BAMS-D-14-00176.1

Şahin S, Türkeş M, Wang SH, Hannah D, Eastwood W (2015) Large scale moisture flux characteristics of the Mediterranean basin and their relationships with drier and wetter climate conditions. Clim Dyn 45:3381–3401. https://doi.org/10.1007/s00382-015-2545-x

Serrano A, García J, Mateos VL, Cancillo ML, Garrido J (1999) Monthly modes of variation of precipitation over the Iberian Peninsula. J Clim 12(9):2894–2919. https://doi.org/10.1175/1520-0442(1999)012%3C2894:MMOVOP%3E2.0.CO;2

Serrano-Notivoli R, Beguería S, Saz MA, Longares LA, de Luis M (2017) SPREAD: a high-resolution daily gridded precipitation dataset for Spain-an extreme events frequency and intensity overview. Earth Syst Sci Data 9(2):721–738. https://doi.org/10.5194/essd-9-721-2017

Seth A, Giorgi F (1998) The effects of domain choice on summer precipitation simulation and sensitivity in a regional climate model. J Clim 11:2698–2712. https://doi.org/10.1175/1520-0442(1998)011%3C2698:TEODCO%3E2.0.CO;2

Sevruk B (1985) Correction of precipitation measurements. In: Proc workshop on the correction of precipitation measurements. WMO/IAHS/ETH, Zürich, pp 13–13

Shahi NK, Das S, Ghosh S, Maharana P, Rai S (2021) Projected changes in the mean and intra-seasonal variability of the Indian summer monsoon in the RegCM CORDEX-CORE simulations under higher warming conditions. Clim Dyn. https://doi.org/10.1007/s00382-021-05771-3

Skamarock WC, Klemp JB, Dudhia J, Gill DO, Barker DM, Duda MG, Huang X-Y, Wang W, Powers JG (2008) A description of the advanced research WRF Version 3. NCAR Technical Notes NCAR/TN-475+STR. https://doi.org/10.5065/D68S4MVH

Taylor KE (2001) Summarizing multiple aspects of model performance in single diagram. J Geophys Res Atmos 106(D7):7183–7192. https://doi.org/10.1029/2000JD900719

Torma C, Giorgi F, Coppola E (2015) Added value of regional climate modeling over areas characterized by complex terrain-Precipitation over the Alps. J Geophys Res Atmos 120:3957–3972. https://doi.org/10.1002/2014JD022781

Trigo RM, DaCamara CC (2000) Circulation weather types and their influence on the precipitation regime in Portugal. Int J Climatol 20(13):1559–1581. https://doi.org/10.1002/1097-0088(20001115)20:13%3C1559::AID-JOC555%3E3.0.CO;2-5

Türkeş M, Erlat E (2006) Influences of the North Atlantic Oscillation on precipitation variability and changes in Turkey. Geophys Space Phys 29:117–135. https://doi.org/10.1393/ncc/i2005-10228-8

Vicente-Serrano SM, López-Moreno JI (2006) The influence of atmospheric circulation at different spatial scales on winter drought variability through a semi-arid climatic gradient in Northeast Spain. Int J Climatol 26(11):1427–1453. https://doi.org/10.1002/joc.1387

Warner TT, Peterson RA, Treadon RE (1997) A tutorial on lateral boundary conditions as a basic and potentially serious limitation to regional numerical weather prediction. Bull Am Meteorol Soc 78(11):2599–2618. https://doi.org/10.1175/1520-0477(1997)078%3C2599:ATOLBC%3E2.0.CO;2

Warrach-Sagi K, Schwitalla T, Wulfmeyer V, Bauer H-S (2013) Evaluation of a climate simulation in Europe based on the WRF–NOAH model system: precipitation in Germany. Clim Dyn 41:755–774. https://doi.org/10.1007/s00382-013-1727-7

Weisman ML, Skamarock WC, Klemp JB (1997) The resolution dependence of explicitly modeled convective systems. Mon Weather Rev 125(4):527–548. https://doi.org/10.1175/1520-0493(1997)125%3C0527:TRDOEM%3E2.0.CO;2

Willmott CJ (1982) Some comments on the evaluation of model performance. Bull Am Meteorol Soc 63:1309–1313

Wu W, Lynch AH, Rivers A (2005) Estimating the uncertainty in a regional climate model related to initial and lateral boundary conditions. J Clim 18(7):917–933. https://doi.org/10.1175/JCLI-3293.1

Zhou X, Yang K, Ouyang L, Wang Y, Jiang Y, Li X, Chen D, Prein A (2021) Added value of kilometer-scale modeling over the third pole region: a CORDEX-CPTP pilot study. Clim Dyn. https://doi.org/10.1007/s00382-021-05653-8

Zittis G, Bruggeman A, Camera C, Hadjinicolaou P, Lelieveld J (2017) The added value of convection permitting simulations of extreme precipitation events over the eastern mediterranean. Atmos Res 191:20–33. https://doi.org/10.1016/j.atmosres.2017.03.002